UNIVERSIDAD NACIONAL AUTÓNOMA DE MÉXICO

PROGRAMA DE POSGRADO EN ASTROFÍSICA

ASTROFÍSICA TEÓRICA

AN ANALYSIS OF THE SSC (SYNCHROTRON SELF-COMPTON) MODEL FOR X-RAY AND GAMMA-RAY EMISSION IN BLAZARS AND ITS IMPLICATIONS

TESIS

QUE PARA OPTAR POR EL GRADO DE:

MAESTRO EN CIENCIAS (ASTROFÍSICA)

PRESENTA:

JAMIE MARLEN AGUILAR MURILLO

DIRECTORES DE TESIS:

DRA. MARÍA MAGDALENA GONZÁLEZ SÁNCHEZ

DR. NISSIM ILLICH FRAIJA CABRERA

INSTITUTO DE ASTRONOMÍA, UNAM, CAMPUS C.U.

MIEMBROS DEL COMITÉ TUTOR

DRA. MARIANA CANO DÍAZ

DR. ANTONIO PEIMBERT TORRES

DR. ALDO ARMANDO RODRÍGUEZ PUEBLA

INSTITUTO DE ASTRONOMÍA, UNAM, CAMPUS C.U.

CIUDAD UNIVERSITARIA, CD. MX, ENERO 2022

Acknowledgements

This research was financially supported by ***Programa de Apoyo a Proyectos de Investigación e Innovación Tecnológica (PAPIIT) AG-100317, IN106521 and IG101320***.

I would like to acknowledge and give my thanks to my supervisors Magda and Nissim who made this work possible. I would also like to thank the examining committee for all the comments and suggestions. I would like to thank the Consejo Nacional de Ciencia y Tecnología (CONACyT) for the financial aid, the Instituto de Astronomía and the UNAM, for all the resources and opportunities granted, that allowed the culmination of this work.

I would like to thank my parents for all the advices and all the sacrifices they made to give me a great education. A special thanks to my mom for all the support and love. I would like to thank all the friends that handed me a helping hand through the whole undergrad and grad experience and specially through life's ups and downs.

I would like to give special thanks to my spouse Lloret Gironés for supporting me through all the hardships of life and always believing in me. Thank you for taking care of me through all those sleepless and stressful nights of research. Your unconditional support and understanding held me up when I couldn't, without your kind words of love and support I wouldn't have made it this far. I couldn't have asked for a better partner in life.

Resumen

En esta tesis abordamos el estudio de la emisión de rayos-X y rayos-γ de los blazares BL Lacs. Proponiendo un modelo leptónico del jet con factor de Lorentz Γ, que contiene un campo magnético, B, constante y una región de emisión llena de electrones relativistas, la cual asumimos que es esférica de radio r_d. Se propone que el jet esté produciendo dichas emisiones mediante un proceso de sincrotrón self Compton (SSC), lo que quiere decir que los electrones que emiten radiación por proceso sincrotrón, correponden a la misma población que por efecto de compton inverso sede energía a los fotones de sincrotrón. Tomamos como fuente de estudio Mkr 421, consideramos el estudio hecho por [González, M. M 2019] en el cual concluyen que las emisiones de rayos X y rayos γ están correlacionados y que dicha correlación es congruente con un model SSC y es capaz de reproducir los flujos observados [Acciari, V. A., 2014] mediante el incremento de la densidad de electrones, sin un cambio en el valor de B. Tomamos dicha conclusión y la ponemos a prueba con el modelo explicado en esta tesis. Se prueba que para correlaciones bajas el espacio de parámetros (B y la densidad de electrones) que es capaz de reproducir dichos flujos es amplio y a medida que la correlación se vuelve mas pronunciada los valores de campo magnético que describen los flujos altos disminuye. Se prueba que la conclusión de [González, M. M 2019] no se mantiene cierta ya que para correlaciones mas pronunciadas el valor del campo magnético debe disminuir para ser capaz de reproducir los flujos altos. Para futuros trabajos se espera poder usar el modelo presentado en esta tesis para estudiar un grupo de BL Lacs y de tal manera entender mejor la física de los BL Lacs y probar si cada blazar tiene un campo magnético dado o si

estos mostrarán correlación siempre.

Abbrevations and Acronyms

AGN	Active Galactic Nucleus
AGNs	Active Galactic Nuclei
BH	Black Hole
BL Lac	BL Lacertae
BLR	Broad Line Region
CMB	Cosmic Microwave Background
EC	External Compton
EGRET	Energetic Gamma-Ray Experiment Telescope
FSRQ	Flat Spectrum Radio Quasars
HBL	High-frequency Peaked BL Lacs
LBL	Low-frequency Peaked BL Lacs
Mkr	Markarian
NLR	Narrow Line Region
SC	Self-Compton
SPB	Synchrotron Proton Blazar

SSC Synchrotron Self-Compton

VHE Very High Energy

Contents

List of Figures

List of Tables

Chapter 1

Introduction

In this chapter I will review some concepts about Active Galactic Nucleus (AGN) needed to later understand the model presented in this thesis. Active Galactic Nuclei (AGNs) are energetic astrophysical sources powered by accretion onto black holes (BH) in galaxies, and they radiate across the full electromagnetic spectrum, from radio to γ-rays.[Padovani, P. 2017]

1.1 Main components

In this section I will introduce some of the main components of AGNs so it serves as tool for understanding of the main interest of this thesis.

Black Hole

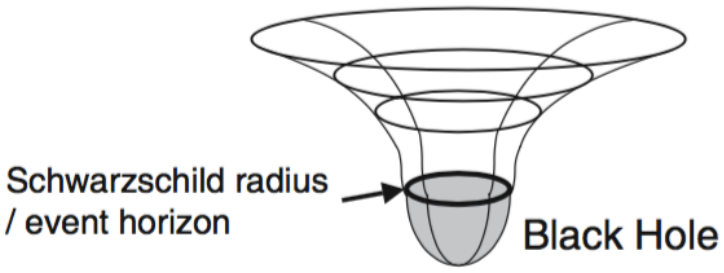

Figure 1.1: Representation of the gravitational potential of a non rotating BH, taken from [Beckmann V. 2012].

Black holes posses such high masses so that their gravitational pull is so strong to allow the escape of light. One of the basic characteristics of a BH is the presence of an event horizon, which is a boundary where matter and light fall inward towards the BH, but never come back out.[Salpeter, E., 1964, Zeldovich, Ya. B., 1964, Lynden-Bell, D. 1969] [Schwarzchild, K. 1916] , described the gravitational field near a non rotating BH in the context of Einstein's theory of General relativity. His solution described the event horizon as a spherical surface centered on the BH. This surface is determined by Schwarzschild radius, as seen in figure 1.1. Any event within the boundary defined by Schwarzschild radius (R_s), will not be able to communicate with an outside observer. [Schwarzchild, K. 1916]

$$R_s = \frac{2GM_{BH}}{c^2}, \tag{1.1}$$

where G is the gravitational constant, c the speed of light in the vacuum, and M_{BH} the BH's mass. [Schwarzchild, K. 1916]

The Kerr metric describes the space time geometry in the vicinity of a rotating massive object such as the central BH of an AGN. Rotating black holes are formed in the gravitational collapse of a collection of stars or gas, which would most likely have nonzero angular momentum.[Blandford, Znajek 1977]

Accretion disk

Accretion disks in galactic centers are formed naturally by in-falling gas that sinks into the central plane of the galaxy, while retaining most of its angular momentum. The assumption is that the viscosity in the disk is enough to provide the needed mechanism to transfer outward angular momentum of the gas to allow it to spiral into the center, losing a considerable fraction of its gravitational energy on the way. The energy lost in the process can be converted into electromagnetic radiation, with extremely high efficiency.[Netzer, H. 2013].

Narrow Line Region

The Narrow line Region (NLR) is located at 100 pc up to kpc scales from the BH. It is biconial shaped region with low velocity gas (<900km/s). The radiation that passes through the NLR produces permitted and forbidden narrow lines in the optical to UV band [Malizia, A. 2020].

Broad Line Region

The Broad line Region (BLR) is about the 0.1-1 pc scale from the BH. This region is made up of high velocity gas (1000-5000km/s). The radiation that passes through the BLR produces permitted broad emission lines in the optical spectra.[Malizia, A. 2020]

Torus

The torus located at a distance of 1 to 100 pc from the BH, is made up of gas and dust. It is responsible for the absorption of the the continuum. It may be as thick to be capable of

hiding the emission up to several keVs. [Malizia, A. 2020]

Jet

The interaction between the BH's magnetic field and the accretion disc may create powerful magnetic jets that eject material perpendicular to the disc at relativistic speeds and extend for hundreds to thousands of parsecs.[Malizia, A. 2020] We will discuss this component with more detail later on.

The components mentioned added up over the years to contribute to the understanding of a large variety of AGN classes at all wavebands and led to the Unified Model of AGN.[Malizia, A. 2020][Urry, M.; Padovani, P. 1995]

1.2 Unified Model

The unified model hypothesises that the diversity of AGN can be explained as a viewing angle effect. An AGN have been classified as radio loud or radio quiet, this according to its emission at radio frequencies, which may be strong or weak [Malizia, A. 2020]. Yet [Padovani, P. 2017] considers this radio loudness classification as obsolete, misleading and inappropriate and instead divides them in terms of jetted and non-jetted, referring to the presence of the jet or lack of it. In this thesis I will consider the radio loudness classification.

Blazars considering the radio loudness classification [Malizia, A. 2020] are considered radio loud AGNs and jetted [Padovani, P. 2017].

Radio loudness	AGN type	Subtype
Radio loud		
	Radio Galaxy	FR I
		FR II
	Quasar	Type 1
		Type 2
	Blazar	
		FSRQ
		BL Lacs
Radio quiet		
	Seyfert	Type 1
		Type 2

Table 1.1: Types of AGNs [Malizia, A. 2020]

1.3 Blazars

Blazars host a jet oriented at a small angle ($\lesssim 15$ - 20°) with respect to the line of sight.Blazars spectra extend over a broad range of energies, from radio to TeV γ-rays. The blazar type is made up of Flat Spectrum Radio Quasars (FSRQs) and BL Lacs. The main difference of these two sub-classes lies in their optical spectra. FSQRs show strong broad emission lines. BL Lacs show at most weak emission lines, sometimes they show absorption features, and in many situations they are completely featureless. To understand the nature of blazars we must understand the nature of their jet. [Urry, M.; Padovani, P. 1995] [Padovani, P. 2017]

The spectral energy distribution (SED) of blazars is characterized by a non-thermal continuum that extends from radio to very high energy γ-rays. They also show a thermal emission in optical/UV which is associated to the accretion disk, and emission lines from the BLR. The dominant emissions are non thermal which are due to the relativist jet. The SED is made up of two distinguishable radiative components due to the jet: the first one peaks

from infrared to X-rays, the second one peaks in the γ-ray band, from MeVs to TeVs. This implies a population of particles that can radiate photons over the electromagnetic spectrum [Cerruti, M. 2020].

1.4 Relativistic Blazar Jet

Blazars have their jet pointing close to our line of sight. The relatavistic jet is moving towards the observer with speed βc, Lorentz factor Γ, therefore it will appear in the observer's frame as showing a projected superluminal motion speed $\beta_{projected} > 1$. Also the emission from the jet is boosted in the direction of the movement which mean that the flux density in the observer's frame scales as $F_v = \delta_D^3 F'_{v'}$ where δ_D is the Doppler factor. [Hovatta, T., Linfords, E. 2020, Cerruti, M. 2020] According to theoretical models jets are magnetically dominated [Blandford, Znajek 1977, Hovatta, T., Linfords, E. 2020]. For blazar γ-ray jets, there are two general ideas, the leptonic and hadronic jet models [Netzer, H. 2013]. Leptonic radiative processes are the ones associated with electrons/positrons while hadronic radiative processes are the ones associated with protons and nuclei. We consider that there exists an efficient particle accelerator in the jet [Cerruti, M. 2020].

Leptonic blazar jet models describe that they have a accretion disk around a BH which powers the jet. Occasionally emitting regions (also known as blobs) of ultrarelativistic electrons are ejected at relativistic bulk velocity. Synchrotron radiation is produced by charged particles moving in a magnetic field. For simplicity it is assumed that the emitting region or blob is a sphere of radius R in the jet, moving with bulk Lorentz factor Γ, and with a homogeneous magnetic field B [Böttcher, M., 2001, Hovatta, T., Linfords, E. 2020, Cerruti, M. 2020, Böttcher, M. 2013]. Leptonic models explain the SEDs high energy component as originated by inverse Compton emission of high energy electrons that scatter off lower energy photons. Some possible target photon fields for Compton scattering are the synchrotron photons produced within the jet, Synchrotron Self-Compton (SSC) mechanisms

[Bloom, S. 1996, Marscher, A. P. 1985, Maraschi, L. 1992, Tavecchio, F. 1998 , Lindfors, E. J 2005, Graff, P. 2008], external photons from the disk(through external Compton (EC) [Dermer, C. D. 1992, Dermer, C. 1993]), EC from the cosmic microwave background (CMB) [Harris, D. E. 2002] and other EC sources [Blazéjowski M. 2000, Arbeiter, C 2002].

For the hadronic jet models we consider, a jet with a blob in which there are also protons.[Sikora, M., 2011, Böttcher, M. 2013] Several works explain the SED of blazars through hadronic models. Protons may contribute through the radiative output of jets in blazars through proton synchrotron emission [Mannheim, K. 1993, Mücke, A. P., Protheroe, R.J. 2001, Aharonian, A. 2000, Mücke, A., Protheroe, R. 2003][Böttcher, M. 2013] or through photo-pion production [Mannheim, K. 1989] [Böttcher, M. 2013, Sikora, M., 2011]. The emission by protons is suppressed and needs to be compensated by a higher magnetic field values, the particle density or both. [Sikora, M., 2011, Hovatta, T., Linfords, E. 2020, Cerruti, M. 2020]

1.5 Hadronic Models

Hadronic models rely on the existence of relativistic hadron populations, located in an emitting magnetized blob, which moves at relativistic speeds along the jet axis. Electron and proton populations are being co-accelerated. The emissions are related to proton-photon interaction ($p\gamma$), either with photons due to external sources, or photons of the same blob. Other processes to consider, depending on the model, are synchrotron due to the co-accelerated electrons or/and protons and other decay mechanisms due to different hadron's decay interactions.

I will review a few concepts for a better understanding of the models described in this section and the following ones. Let's start by defining which particles are hadrons and which are leptons as shown in table 1.2 and 1.3. As shown in figures 1.2 and 1.3, when

a proton interacts with a high energy photon, the interaction (known as pγ) may lead to the production of additional hadrons. Perhaps to neutral pion, as seen in figure 1.2, which may in turn decay. Its primary or dominant decay channel is into two photons. Photons primarily interact with matter via pair production, i.e. electron e^- and positron e^+ pairs. This production will continue as long as the photon interacts with a nucleus, and has an energy above the total rest mass energy of the two particles produced. In turn, electron-positron annihilation may occur.[Bettini, A. 2008]

Leptons			
Charged	electron e	muon μ	tau τ
Neutral	electron neutrino ν_e	muon neutrino ν_μ	tau neutrino ν_τ

Table 1.2: Lepton flavors [Bettini, A. 2008].

Hadrons		
Byrons	Protons p	neutrons n
Mesons	Pions π	kaons K

Table 1.3: Hadron types [Bettini, A. 2008].

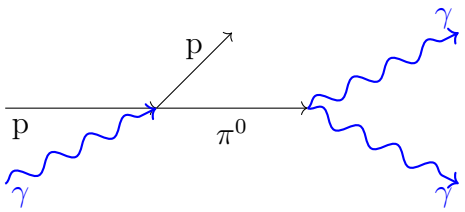

Figure 1.2: Proton(p) photon (γ) interaction, neutral pion (π^0) decay.

Through the deceleration of a charged particle, the loss of kinetic energy is converted into radiation. $p\gamma$ interactions produce a charged pion, as seen in figure 1.3, and the primary decay channel of a charged pion, $\pi^{\pm}$, is into a muon, $\mu^{\pm}$, and muon neutrino, ν_μ, ($\pi^+ \longrightarrow$

$\mu^+ + \nu_\mu$, $\pi^- \longrightarrow \mu^- + \bar{\nu_\mu}$). Which, in turn, the primary decay channel of charged muons, $\mu^\pm$, is into an electron, e^-, electron neutrino, ν_e, and a muon neutrino, ν_μ, ($\mu^- \longrightarrow e^- + \bar{\nu_e} + \nu_\mu$, $\mu^+ \longrightarrow e^+ + \nu_e + \bar{\nu_\mu}$).[Bettini, A. 2008]

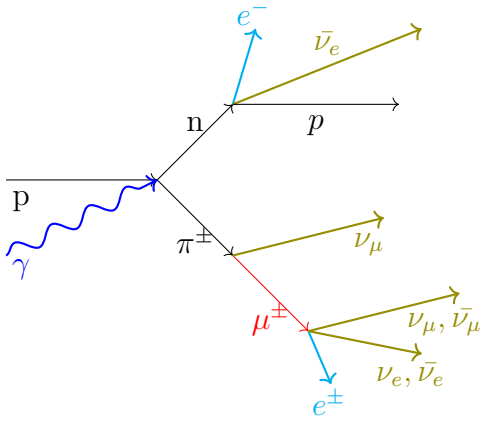

Figure 1.3: Proton photon interaction, charged pion decay and the following primary decay channels.

[Mücke, A. P., Protheroe, R.J. 2001] proposed a synchrotron proton blazar (SPB) model where the high-energy bump of the SED is due to accelerated protons, while the low energy bump is due to synchrotron radiation by co-accelerated electrons. It is assumed that the relativistic e^- radiate synchrotron photons, which serve as target radiation field for pγ interactions, and for the subsequent pair-synchrotron cascade, which develops due to photon-photon pair production. Using Monte Carlo technique to simulate the interactions and subsequent cascades, it was possible to fit the high-energy portion of the observed SED of Markarian (Mrk) 501, during the April 1997 flare. In the model for Mkr 501, synchrotron radiation from protons in a highly magnetized emission region are responsible for the TeV bump, while the X-ray bump mainly by the synchrotron radiation from the accelerated electrons. If the optical depth of TeV photons is significantly higher, a corresponding amount may be redistributed to X-ray energies.

[Mücke, A., Protheroe, R. 2003] presented a parameter study of the SPB to explain γ-ray loud objects, LBLs (Low-frequency Peaked BL Lacs) and HBLs (High-frequency Peaked

BL Lacs). It was stated that the model needs strong magnetic fields together with proton, muon, pion synchrotron radiation to produce the double bumped SED observed during active phases of γ-ray emission. HBLs' radiation is dominated by proton synchrotron radiation at MeV-TeV energies. In LBLs, besides the proton synchrotron radiation, there is a significant contribution from muon synchrotron radiation at MeV-TeV energies.

Some of the characteristics that hadronic models share is that they mostly need large magnetic fields. Evidence that hadrons contribute to the γ-ray emission would be confirmed with associated neutrino observations, which would rule out purely electromagnetic processes and require for the decay of hadrons. It is possible to have high energy SED component in blazars and proton synchrotron peak frequency at around 10-100 GeV, assuming, magnetic field, $B \simeq 10 - 100$ G, maximum proton Lorentz factor, $\gamma_{p,max} \simeq 10^9$, and Doppler factor, $\delta \simeq 10 - 50$. [Sikora, M., 2011, Hovatta, T., Linfords, E. 2020, Cerruti, M. 2020]

1.6 Leptonic Models

Leptonic models explain the high energy component as originated by inverse Compton emission of high energy electrons that scatter off lower energy photons. Several radiation fields or photons that work as targets for the high energy electrons to scatter have been proposed. For instance, photons produced through synchrotron emission by the same population of electrons, optical, UV, X-ray emission from the central accretion disk, emission from the BLR and the NLR, infrared emission from the torus, and radiation from the cosmic microwave background, just to mention a few of the possible radiation fields that may serve as targets for inverse Compton processes. Other considerations are: a magnetic field with no preferred orientation in the co-moving frame of the emission region, and a spherical emitting region filled up with hot plasma.

In the case where the radiation field that serves as target for inverse Compton scattering is the radiation emitted through synchrotron by the same population of electrons we have the called SSC (Synchrotron Self-Compton) mechanisms.

[Marscher, A. P. 1985] presented models for the variability of compact radio sources, with special interest on the applications for the flare of 3C 273. It was presented that the emissions observed were to be expected if the relativistic electrons responsible for the flare are continuously injected with the same energy distribution as for the quiescent emission and subsequently suffer significant energy losses to synchrotron radiation or Compton scattering. They presented a model based on an uniform expanding source, allowing a variable injection of relativistic electrons and magnetic field and including synchrotron, Compton, and expansion losses which could reproduce the observed behavior of 3C 273, if the injection is allowed to vary with radius.

Since the nature of the uniform expanding source model did not seem to fill the expectations, they tried a different approach. They adopted a physical model of the source and determined whether the temporal behavior of the model fulfills the observations. So they chose a model in which the jet is conical, directed nearly along the line of sight, with constant opening and with relativistic electrons and a magnetic field injected at a point which lies at an axial distance from the vertex. Any increase in the pressure of the jet flow will result in the formation of a shock. The electrons gain energy at a constant rate as they cross the shock. They found that an important consequence of a shocked region in a relativistic jet is a variable self-Compton X-ray and γ-ray emission. Nevertheless, the approach is an approximate. The Compton spectrum is quite sensitive to uncertainties in the physical parameters. They stated that Compton losses during the initial stages of the flare indicates that Compton scattering may produce the observed X-ray and γ-rays. The model produces several observationally testable predictions, such as that of 1983 flare in 3C 273.

[Maraschi, L. 1992] studied the blazar 3C 279 through a model in which they assumed

that X-rays and γ-rays are produced in the same region by relativistic electrons that interacting with a magnetic field radiate photons that through inverse Compton produce γ-rays. In this model, γ-ray luminosity is higher than the emitted at lower frequencies, produced by synchrotron processes, therefore, the radiation energy density is higher than the magnetic energy density. From the maximum observed radiation on blazar 3C 279, they inferred that synchrotron processes would produce the observed UV and soft-X-ray photons. The shape of the jet proposed is parabolic in the inner part and conical in the outer parts. For simplicity, the emitting region is homogeneous and spherical and in the source frame photons are isotropically distributed. The considered size of the γ-ray emitting region is inconsistent with the variability time scale of 2 days. Bulk acceleration of the plasma occurs in the inner parabolic part of the jet, where the bulk Lorentz factor increases with distance. In the hard X-ray and γ-ray band, only the inner portions of the jet contribute. In the 'high-state', the synchrotron emission steepens from infrared to UV band and the inverse Compton from the hard X-ray to the γ-ray band. In the observed 'low-state', the Compton component, predicted with the model, falls above the lowest X-ray, data which may be due to the lack of simultaneous observations. They concluded that for emitting regions of up to 2×10^{17} cm and Lorentz factors between 5.5 and 14, the model is more accurate.

[Bloom, S. 1996], due to detection of γ-ray energies > 100 MeV, stated that it was necessary to reconsider models to link the radio to optical emission to X-ray and γ-ray emission. In their model, they presented a component due to synchrotron emission and a first and second order self-Compton component, the component due to inverse scattering. Their main goal was to explore the dependence of the broadband spectra on physical parameters, in order understand the observed variability in terms of parameters such as magnetic field, B, and electron density, N_e, and other parameters. They considered a simple model for the synchrotron radiation, and did not considered expansion, energy losses, relativistic time delay, particle acceleration, etc.

Without modeling the causes for variability, they examined how synchrotron and

self-Compton components vary with the magnetic field, source size, electron density and electron energies using the common expressions to determine the values of B and N_e in terms of the observable parameters. They developed a numerical program that generates synchrotron and inverse Compton spectra, finding that, when the magnetic field changes, both the synchrotron and the self-Compton component flux densities increase. When varying R in the interval $[6.5\times10^{17}, 1.3\times10^{18}, 2.6\times10^{18}]cm$, there is an increase in the scattered flux, as expected since it increases with volume as R^3. Varying electron upper cutoff energy, γ_2 , causes synchrotron and scattered spectra to extend to higher frequencies. Varying electron lower cutoff energy γ_1, does not have much effect on the X-ray emission but the self Compton flux is higher at optical frequencies. Keeping the product of N_e and R constant, has an effect similar to that of an increase in B, except that the upper cutoff energies remain constant. N_e causes X-ray and γ-ray flux densities to vary by larger fractions. This contrasts with models where γ results from photons external to the jet. According to EGRET-detected blazar, the second order SCC is not an important contributor, but there is a contribution seen in some observations. Their SSC model and their analytical considerations provide a formulation to relate the variability of the high energy spectra to that of the radio-IR emission. The second order self-Compton scattering tends to dominate the γ-ray emission in sources with steeper spectral indices, first order SSC emission remains as the main candidate to explain the hard γ-rays observed in sources.

[Tavecchio, F. 1998] proposed a model assuming a spherical, filled with relativistic electrons and a magnetic field with no preferred direction and the energy distribution of the electrons following as broken power law. With the source transparent to γ-rays, the high energy photons may interact with the low energy photons, producing pairs explaining the time lags with the hypothesis that they are associated to the time necessary for freshly high energy electrons to cool. The break energy and the two spectral indices are determined through observed spectra. The cooling is considered as dominated by synchrotron processes and the break in energy results from a balance between the cooling time and the escape time. The soft photon lags observed in some sources are explained by radiative cooling of high energy particles. It was showed that the constraints lead to equations that can be

expressed in terms of the magnetic field and the Doppler factor. The value found for the magnetic field intensity and Doppler factor for Mkr 501 are ~ 0.3 G and ~ 10, respectively. For two sources, Mrk 421 and PKS 2155-304, the derived parameters were a Doppler factor ~ 25 and a magnetic field $B \sim 0.2$ G.

[Lindfors, E. J 2005] took into account a SSC model for the observed SEDs of 3C 279, considering the inverse Compton maximum to be in the γ-ray energy range. The Doppler boosting factor has to be high for inverse Compton and, in the external Compton mechanisms, the magnetic fields need to be strong, and also the luminosity of the external photon field has to be high. So, they present a multi component scenario, where the synchrotron emission originates from both the jet and from the shocks propagating downstream in the jet. From observed time delays from radio to γ-ray flares, they estimated that the shock are at distances of a several parsec from the jet apex. Beyond the BLR, they may not be enough external photons to produce a significant external Compton radiation. They found that with the size, Doppler boosting and the variability time scale constraints, the SSC model cannot reproduce all the high energy flux in quiescent or high states, even though the fits show that X-ray emission may be plausible to be reproduced by the shocks.

[Dermer, C. D. 1992] proposed an EC model with Compton scattering of accretion disk photons by relativistic non-thermal electrons in the jet. The accretion disk source and the core of the AGN emit target photons isotropically, photons passing through the blob follow trajectories parallel to the jet axis. [Dermer, C. 1993] proposed an EC from the disk as well and angle dependence. Photons that enter the jet from the side, can make more important contributions to the loss rate than luminous emission emitted from the innermost regions of the supermassive BH. Photons that interact at large angles with respect to the jet axis, dominate the electron energy loss rate in the comoving fluid frame. The Compton scattering energy loss rate of the relativistic electrons in the blob is mainly due to accretion disk photons, rather than scattered photons at distances $\lesssim 0.01 - 0.1$pc from the central source. This eliminates the need to call upon different source models for quasars and BL Lac objects, for this to be true BL Lacs would be viewed as weak quasars, with no emission

lines.

[Blazéjowski M. 2000] assumed relativistic electrons/positrons enclosed within a very thin shell that propagates along the jet where energy losses are due to synchrotron, Compton scattering of synchrotron radiation and Compton scattering of external radiation. Three cases are considered, one, where the γ-rays are produced by Comptonization of near-IR radiation, other, due to Comptonization of the broad line region and the last, as a combination of both. An electron/positron injection function as a power law injected at a constant rate. It is assumed that the shell propagates at a constant Lorentz factor. The model approximates a situation in which the shell containing relativistic plasma is formed as a result of the collision of two perturbations moving down the jet at different speeds. Near-infrared Comptonization (model A) yields spectra smoother and closer to the observed ones, than the spectra produced by BLR Comptonization (model B). Lorentz factors for electrons where the cooling break occurs need to be larger for model A than in model B, causing the X-ray portion of the SSC component to be harder in model A, compared to model B. In the γ-ray spectral band, the spectral component, due to IR, has a break at $\sim$1 GeV, whereas in observations from EGRET/CGRO blazar spectra extend to at least 5 GeV. Therefore, the EGRET spectra can be produced only by the combination of IR and BLR components. This also provides an interesting explanation for γ-ray spectra being steeper than the X-ray spectra. According to Blazéjowski, Comptonization of infrared radiation produced by hot dust should be taken into account in all radiation models of blazars, since such radiation is likely to be present in quasar cores at parsec scales, where it is sufficiently dense to compete with BLR flux, as the source of Compton cooling. If blazar radiation is produced at distances larger than the distance at which energy density of the BLR light peaks, the IR component is expected to dominate over the BLR component. EC models predict the general steepening of the γ-ray and synchrotron spectra with energy in qualitative agreement with observations. However, the lower observed variability amplitude of synchrotron flux compared with γ-ray flux suggests contamination of synchrotron radiation produced at larger distances or stationary shocks. The X-ray spectrum would be a superposition by the SSC component and the harder EC component.

[Arbeiter, C] considers EC from both the dust torus and the accretion disk, stating that for small angles to the jet axis and distances of more than a few accretion disk radii the dust surrounding the AGN is more important as target photon source for inverse-Compton scattering. [Harris, D. E. 2002] suggested an EC contribution from cosmic microwave background (CMB) photons. Inverse Compton emission from the relativistic electrons scattering off the CMB is incapable of producing the observed intensity of X-rays, unless relativistic effects that modify the apparent luminosity are considered. Finding that this model is favored by higher redshifts and steeper radio spectra, while local sources with flatter radio spectra are most likely dominated by synchrotron emission.

1.7 Blazars with Correlation of the X-ray and γ-ray Emission

Several multiwavelength observations for several blazars have been performed to identify the emission mechanisms and to constrain the parameters describing the emission in blazar jets. In one zone leptonic models, we would expect that the emission at different wavelength to be correlated when produced essentially by the same electron population. V. Acciari (2014) [Acciari, V. A., 2014] studied observations of Markarian 421 over a span of 14 years with TeV energies observations from Whipple (December 1995 to May 2009) and from VERITAS. They correlated Whipple observations with data taken at other wavelengths for part or all of the epoch 1995-2009. The most complete overlap was with Rossi X-ray Timing Explorer (RXTE) database for the entire 14 years. RXTE had three non-imaging X-ray detectors, one of which is the All-Sky Monitor (ASM). The RXTE ASM data for the epoch show evidence for emission correlated with γ-ray data on monthly and yearly timescales. The correlation coefficients for monthly-binned data is r_c=0.75 and for yearly-binned date is r_c=0.89. The strong correlation suggests that the X-rays and γ-rays are emitted by the same population of electrons in the same region of the jet. Yet other wavelengths (radio, optical, infrared)

are not strongly correlated.

[Rachen Jörg P. 2001] found from simultaneous multiwavelength observations of Mrk 421 and Mrk 501, that their variability in the X-ray and γ-ray regime is largely correlated and stronger than in other bands. Which would serve as an argument against hadronic models. [Gutierrez, K 2006] studied the multiwavelength observation campaign of blazar 1ES 1959+650, May 2003 to June 7 and compared the source characteristics with those measured during observations taken during previous years. They found correlation between the simultaneously measured TeV γ-ray and X-ray fluxes during the 2002 and 2003 observation campaigns. Both, the fluxes and photon indices, appear to be correlated for the 2002 data set. The lack of a correlation between the high energy (X-ray and γ-ray) and low energy (radio and optical) flux levels observed in the years 2002 and 2003 suggests that the high energy radiation is produced close to the central engine and that the low energy radiation is produced farther downstream of the jet. [Tachibana, Y. 2014] studied the data in optical, X-ray and γ-ray bands for blazar 3C 454.3. Variation, especially activities like flares, are seen to be completely correlated across the three energy bands. In terms of the flare amplitudes the X-ray band seems to show lower variabilities than the optical and γ-ray bands. [González, M. M 2019] used a maximum likelihood approach to estimate the monthly robustness in Whipple-RXTE/ASM correlation for Mkn 421.

Considering the correlations found on several blazars, it is plausible to consider that mechanisms behind the X-ray and γ-ray emission on blazars are due to one zone leptonic models. So far, different models have been constructed to explain the observed emissions, both leptonic and hadronic. Within these models that were mentioned earlier, the TeV orphan flare remains either as an open question or explained as a whole new phenomena. Using [González, M. M 2019] considerations for the correlation for Mkn 421, a model is proposed to explain the X-ray and γ-ray emission of blazars as one physical process dependent of parameters, whether they are in quiescent, flaring state or presenting Tev orphan flares.

Chapter 2

Synchrotron Self-Compton Model

As an attempt for a better understanding of blazars hence their physical properties, in this thesis we propose a SSC model. Before taking this task we undertook the task of studying the existing models mentioned in the previous chapter. Mkr 421 [Sikora, M. 2000], is one of the closest and brightest therefore serves as a good study source, observations [Macomb, D. J 1995, Fossati, G. 2008, Acciari, V. A 2011, Aleksić, J. 2015, Aleksić, J 2015, Baloković, M. 2016, Acciari, V. A., 2014] suggest correlation between the X-ray and γ-ray emissions, this may be interpreted well in a SSC model.

In this chapter, I will discuss the a one zone synchrotron self-Compton model proposed in this thesis. We consider a leptonic jet model which will depend on four parameters, electron density N_e,constant magnetic field B,a bulk Lorentz factor Γ and radius r_d. We consider an emitting region (blob) as an sphere for simplicity with a radius r_d and it is filled with a relativistic electron density N_e, which is moving towards the observer with a bulk Lorentz factor Γ, and filled with a homogeneous, constant magnetic field B, as shown in figure 2.1 . Here on we define the universal constants $c = \hbar = 1$ in natural units.

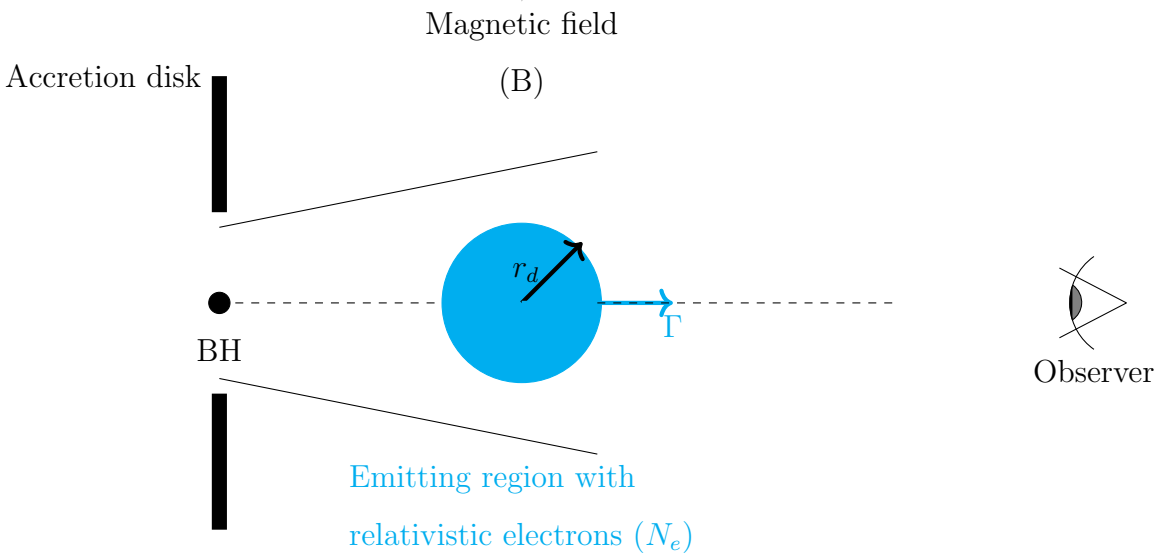

Figure 2.1: A visual representation of the jet model.

2.1 Synchrotron Emission

As we reviewed in (Appendix) 5.1 synchrotron radiation is produced by the interaction of charged particles moving in a magnetic field. If there is a particle with charge q_e and Lorentz factor $\gamma_e = E/m_e$ in the region it would radiate a synchrotron power in he form of equation 5.23. We assume that the blob is made up of more than a single electron, instead is made up of a population of electrons described with a broken power law distribution of Lorentz factor γ_e, defined between $\gamma_{e,m}$ and $\gamma_{e,max}$ as [Longair, 1994],

$$N_e(\gamma_e) = N_{0,e} \begin{cases} \gamma_e^{-\alpha} & \gamma_{e,m} < \gamma_e \leq \gamma_{e,c} \\ \gamma_{e,c}\gamma_e^{-(\alpha+1)} & \gamma_{e,c} < \gamma_e < \gamma_{e,max}. \end{cases} \tag{2.1}$$

Where $N_{0,e}$ is the normalization factor,which is associated to the number density of the electrons in the emission region; α is the power index of the electron distribution; the Lorentz cooling factor ,$\gamma_{e,c}$, which gives the cooling energy, break in energy, of the electron where the slope changes; the minimum and the maximum energy of the electron population given by their respective electron Lorentz factors $\gamma_{e,m}$ and $\gamma_{e,max}$.

2.1.1 Minimum Energy

We assume an equipartition of energy, we have that magnetic energy density is given by $U_B = B^2/8\pi$ and the total electrons energy density is described as,

$$U_e = m_e \int \gamma_e N_e(\gamma_e) d\gamma_e, \tag{2.2}$$

where m_e is the rest electron mass, γ_e is the electron's Lorentz factor and $N_e(\gamma_e)$ is given by equation 2.1. If we consider that a fraction of the total energy density is used to accelerate the electrons we may proceed to find the minimum electron Lorentz factor. We integrate our electron distribution $N_e(\gamma_e) = \int N_e(\gamma'_e) d\gamma'_e$ defined between $\gamma_{e,m}$ and $\gamma_{e,max}$ and for $\alpha > 2$ we find:

$$\boxed{N_e \simeq \frac{N_{0,e}}{\alpha - 1} \gamma_{e,m}^{-\alpha+1}} \quad . \tag{2.3}$$

Solving for the electron energy density given by equation 2.2 for the electron distribution given by equation 2.1 we find:

$$\boxed{U_e \simeq \frac{N_{0,e} m_e}{\alpha - 2} \gamma_{e,m}^{-\alpha+2}} \quad . \tag{2.4}$$

Using 2.3 and 2.4, we may write the minimum electron Lorentz factor in terms of the energy density and the distribution of the electrons. As follows,

$$\boxed{\gamma_{e,m} = \frac{\alpha - 2}{m_e(\alpha - 1)} \frac{U_e}{N_e}} \quad . \tag{2.5}$$

2.1.2 Cooling Energy

As electrons radiate synchrotron photons, they lose energy (cooling energy). The cooling time, t_{cool}, is the time related to the energy loss due to synchrotron radiation. The energy loss per unit of time or the power emitted due to synchrotron is found earlier given by equation 5.14 and keeping in mind the energy of an electron is given by $\epsilon_e = \gamma_e m_e$, we can obtain the

cooling time as [Inoue, S. 1996],

$$t_{cool} = \frac{\epsilon_e}{d\epsilon_e/dt} = \frac{\gamma_e m_e}{\frac{4}{3}\sigma_T \gamma_e^2 U_B} = \frac{3m_e}{4\sigma_T \gamma_e U_B}. \tag{2.6}$$

The blob moves at relativistic velocities with Doppler factor δ_D along the jet in an outwards direction. We consider the dynamic time scale associated with the expansion of the emitting region as it travels along the jet, may also be interpreted from a mathematical point as an energy independent particle escape from the blob , which is defined as [Inoue, S. 1996, Cerruti, M. 2020]:

$$t_d \simeq \frac{r_d}{\delta_D} \quad . \tag{2.7}$$

The electron's cooling Lorentz factor, $\gamma_{e,c}$ satisfies $t_{cool} \simeq t_d$ [Inoue, S. 1996],

$$\frac{3m_e}{4\sigma_T \gamma_{e,c} U_B} = \frac{r_d}{\delta_D} \quad . \tag{2.8}$$

Doing so, we get the cooling electron Lorentz factor as

$$\boxed{\gamma_{e,c} = \frac{3m_e}{4\sigma_T} \delta_D r_d^{-1} U_B^{-1} \quad .} \tag{2.9}$$

2.1.3 Maximum Energy

The blob's electrons must have an energy limit reflecting the acceleration mechanisms taking place. The maximum energy of the electrons is estimated by equating t_{cool} with t_{acc} which is given as [Inoue, S. 1996],

$$t_{acc} = \sqrt{\frac{\pi}{2}} \frac{m_e}{q_e} \gamma_e U_B^{-1/2} = \sqrt{\frac{\pi}{2}} U_B^{-1/2} \frac{\epsilon_e}{q_e} \quad . \tag{2.10}$$

$$t_{acc} \simeq t_{cool} \tag{2.11}$$

$$\sqrt{\frac{\pi}{2}} U_B^{-1/2} \frac{\epsilon_{e,max}}{q_e} = \frac{3m_e^2}{4\sigma_T U_B} \frac{1}{\epsilon_{e,max}} \tag{2.12}$$

$$\epsilon_{e,max} = \left[\frac{9m_e^4 q_e^2}{8\pi\sigma_T}\right]^{\frac{1}{4}} U_B^{-1/4}. \tag{2.13}$$

Now we can write the maximum electron Lorentz factor as,

$$\boxed{\gamma_{e,max} = \left[\sqrt{\frac{\pi}{2}} \frac{3q_e}{4\sigma_T} U_B^{-1/2}\right]^{1/2} \quad .} \tag{2.14}$$

2.1.4 Synchrotron Spectrum

We have that the energy of a photon is given by $\epsilon = h\nu$, photons emitted by synchrotron have $\nu \simeq \frac{\gamma^2 q_e B}{m_e}$, as discussed in Appen. B equation 5.19. The energy of the emitted photons by synchrotron is given by,

$$\boxed{\epsilon_\gamma^{syn} = \frac{\delta_D q_e U_B^{1/2}}{m_e}\sqrt{8\pi}\gamma_e^2 \quad .} \tag{2.15}$$

To find the minimum, cooling, and maximum energy of the emitted photons we take the above equation and substitute the corresponding Lorentz factor.

$$\epsilon_{\gamma,m}^{syn} = \frac{\delta_D q_e U_B^{1/2}}{m_e}\sqrt{8\pi}\gamma_{e,m}^2 \tag{2.16}$$

$$= \frac{\delta_D q_e U_B^{1/2}}{m_e}\sqrt{8\pi}\left[\frac{(\alpha-2)}{m_e(\alpha-1)}\frac{U_e}{N_e}\right]^2 \quad . \tag{2.17}$$

Then the photon's minimum energy is given by:

$$\epsilon_{\gamma,m}^{syn} = \frac{\sqrt{8\pi}(\alpha-2)^2 q_e \delta_D U_B^{1/2} U_e^2}{(\alpha-1)^2 m_e^3 N_e^2} \quad . \tag{2.18}$$

Similarly the photon's cooling energy

$$\epsilon_{\gamma,c}^{syn} = \frac{\delta_D q_e U_B^{1/2}\sqrt{8\pi}}{m_e}\gamma_{e,c}^2 \tag{2.19}$$

$$= \frac{\delta_D q_e U_B^{1/2}\sqrt{8\pi}}{m_e}\left(\frac{3m_e}{4\sigma_T}\delta_D r_d^{-1} U_B^{-1}\right)^2 \quad . \tag{2.20}$$

rearranging, we get

$$\boxed{\epsilon_{\gamma,c}^{syn} = \frac{9 q_e m_e \sqrt{8\pi}}{16\sigma_T^2}\delta_D^3 r_d^{-2} U_B^{-3/2} \quad ,} \tag{2.21}$$

When electrons and photons coexist in a region the repeated scattering of photons will modify their spectrum. When an IC is considered, we include the correction Compton parameter, $\left(1+\frac{U_e}{U_B}\right)$ in $\gamma_{e,c}$ [Rybicki, G. 1986, Sari, R. 2001]

$$\gamma_{e,c} = \frac{3m_e}{4\sigma_T}\delta_D r_d^{-1} U_B^{-1}\left(1+\frac{U_e}{U_B}\right) \quad . \tag{2.22}$$

So then our photon's cooling energy is given by

$$\boxed{\epsilon_{\gamma,c}^{syn} = \frac{9 q_e m_e \sqrt{8\pi}}{16\sigma_T^2}\left(1+\frac{U_e}{U_B}\right)^{-2}\delta_D^3 r_d^{-2} U_B^{-3/2} \quad .} \tag{2.23}$$

Now, calculating the photon's maximum energy

$$\epsilon^{syn}_{\gamma,max} = \frac{\delta_D q_e U_B^{1/2}\sqrt{8\pi}}{m_e^3}\gamma^2_{e,max} \quad , \tag{2.24}$$

$$\epsilon^{syn}_{\gamma,max} = \frac{\delta_D q_e U_B^{1/2}\sqrt{8\pi}}{m_e^3}\sqrt{\frac{2}{\pi}}\frac{3m_e^2 q_e}{4\sigma_T}U_B^{1/2} \quad . \tag{2.25}$$

Thus photon's maximum energy is given by

$$\boxed{\epsilon^{syn}_{\gamma,max} = \frac{3q_e^2}{\sigma_T m_e}\delta_D(1+z)^{-1} \quad .} \tag{2.26}$$

The observed synchrotron spectrum is obtained by the shape of the electron distribution, we may estimate the photon spectrum through emissivity $\epsilon_\gamma N_\gamma(\epsilon_\gamma)d\epsilon_\gamma$; as $\epsilon_\gamma \simeq \langle\epsilon_\gamma\rangle\,\delta(\omega-\omega_c)$ doing as [Rybicki, G. 1986, Longair, 1994] we show that for spectral indices of the electron distribution α and $(\alpha-1)$, we obtain a photon distribution with spectral indices $p=(\alpha-1)/2$ and $p=\alpha/2$, respectively. Therefore photon spectrum, can be written as

$$\left[\epsilon_\gamma^2 N(\epsilon_\gamma)\right]_{\gamma,syn} = A_{\gamma,syn}\begin{cases} \left(\frac{\epsilon_\gamma}{\epsilon^{syn}_{\gamma,m}}\right)^{4/3} & \epsilon_\gamma < \epsilon^{syn}_{\gamma,m} \quad , \\ \left(\frac{\epsilon_\gamma}{\epsilon^{syn}_{\gamma,m}}\right)^{-\frac{\alpha-3}{2}} & \epsilon^{syn}_{\gamma,m} < \epsilon_\gamma < \epsilon^{syn}_{\gamma,c} \quad , \\ \left(\frac{\epsilon^{syn}_{\gamma,c}}{\epsilon^{syn}_{\gamma,m}}\right)^{-\frac{\alpha-3}{2}}\left(\frac{\epsilon_\gamma}{\epsilon_{\gamma,c}}\right)^{-\frac{\alpha-2}{2}} & \epsilon^{syn}_{\gamma,c} < \epsilon_\gamma < \epsilon^{syn}_{\gamma,max} \quad , \end{cases} \tag{2.27}$$

where

$$A_{\gamma,syn} = \frac{4\sigma_T}{9}d_z^2\delta_D^3 U_B r_d^3 N_e \gamma^2_{e,m} \quad . \tag{2.28}$$

$A_{\gamma,syn}$ is the proportionality constant estimated by the product of the total number of radiating electrons in the volume and the maximum radiated power, where d_z is the distance from the source. Equation 2.27 describes the synchrotron spectrum as function of the magnetic field B, the electron density N_e, the size of the emission region r_d, the bulk Lorentz factor Γ and the spectral index α.

2.2 Inverse Compton

Now, we will calculate our photons due to inverse Compton. From now on the primed values signify the electrons' rest frame. In the Appen. B we find the incident photon's energy given

by the equation 5.40 ($\epsilon' = \epsilon\gamma(1 - \beta\cos\theta)$), where $\beta = \frac{v}{c}$ which is the β factor from the Doppler shift and θ is the angle between the electrons trajectory and the photon as seen in the lab frame. If we suppose that photons (which entered at angle θ' in the electrons frame, as seen in figure 5.4, the primed values signify the electrons rest frame) rebound at an angle θ'_1. We say $\theta'_1 - \phi = \theta'$. Using equation 5.34 in the electrons frame:

$$\epsilon'_1 = \frac{\epsilon'}{1 + \frac{\epsilon'}{mc^2}(1 - \cos\phi)} \quad . \tag{2.29}$$

Going back to the lab frame, we have using 5.41 ($\epsilon_1 = \epsilon'_1\gamma(1 + \beta\cos\theta'_1)$). Replacing the ϵ'_1(equation 2.29) on equation 5.41, we have the scatter photon energy as:

$$\epsilon_1 = \frac{\epsilon'\gamma(1 + \beta\cos\theta'_1)}{1 + \frac{\epsilon'}{mc^2}(1 - \cos\phi)} \quad . \tag{2.30}$$

Now replacing 5.40 on 2.30 we have:

$$\epsilon_1 = \frac{\epsilon\gamma^2(1 - \beta\cos\theta)(1 + \beta\cos\theta'_1)}{1 + \frac{\epsilon'}{mc^2}(1 - \cos\phi)} \quad . \tag{2.31}$$

On equation 2.31, I left ϵ' in the denominator, just so it doesn't look so crowded, also we want the limit where $\epsilon' \ll m_e c^2$ and leaving it as it is seems convenient. So, for $\epsilon' \ll m_e c^2$ equation 2.31, turns into $\epsilon_1 \approx \epsilon\gamma^2(1-\beta\cos\theta)(1+\beta\cos\theta'_1)$. In a 'typical' collision $\theta \sim \theta'_1 \sim \frac{\pi}{2}$ so, we get:

$$\epsilon_1 \approx \epsilon\gamma^2. \tag{2.32}$$

To find the energies of the photons due to inverse Compton, we are going to use equation 2.32. In 2.32 ϵ is the incident energy which, in our model will correspond to the energy of photon emitted by synchrotron. Here we denote as $\epsilon_{\gamma,i}$ where i denotes whether if it is cooling, maximum or minimum. So, the inverse Compton photons energy, here we will call it SSC since the seed electrons of both the synchrotron and inverse Compton are from the same population , is given by:

$$\epsilon_\gamma^{SSC} = \gamma_{e,i}^2 \epsilon_{\gamma i}^{syn} \quad , \tag{2.33}$$

where $\gamma_{e,i}^2$ is the corresponding Lorentz factor and $\epsilon_{\gamma i}^{syn}$ is the incident energy of the photon, which is given by the synchrotron photon energies we found earlier. We call it ϵ_γ^{SSC}, since the same electrons that are synchrotron radiating, scatter up their own radiation, which

is known as SSC (sycnrotron self Compton). Using 2.33, we find the energies of radiated photons through inverse Compton. The minimum energy is given by

$$\epsilon_{\gamma,m}^{SSC} = \gamma_{e,m}^2 \epsilon_{\gamma,m}^{syn} \quad . \tag{2.34}$$

The minimum energy is given by

$$\epsilon_{\gamma,m}^{SSC} = \frac{\sqrt{8\pi}(\alpha-2)^4}{(\alpha-1)^2} \frac{q_e \delta_D}{m_e^5} \frac{U_e^4 U_B^{1/2}}{N_e^4} (1+z)^{-1} \quad . \tag{2.35}$$

The maximum energy is given by

$$\epsilon_{\gamma,max}^{SSC} = \frac{9}{4}\sqrt{\frac{2}{\pi}} \frac{q_e^3}{\sigma_T^2 m_e} \delta_D U_B^{-1/2} (1+z)^{-1} \quad . \tag{2.36}$$

The cooling energy is given by

$$\epsilon_{\gamma,c}^{SSC} = \frac{81 q_e m_e^3 \sqrt{8\pi}}{256 \sigma_T^4} \delta_D^5 r_d^{-4} \left(1 + \frac{U_e}{U_B}\right)^{-4} U_B^{-7/2} (1+z)^{-1}. \tag{2.37}$$

The Compton scattering spectrum obtained as a function of the synchrotron spectrum is

$$\left[\epsilon_\gamma^2 N(\epsilon_\gamma)\right]_{\gamma,SSC} = A_{\gamma,SSC} \begin{cases} \left(\frac{\epsilon_\gamma}{\epsilon_{\gamma,m}^{SSC}}\right)^{4/3} & \epsilon_\gamma < \epsilon_{\gamma,m}^{SSC} \quad , \\ \left(\frac{\epsilon_\gamma}{\epsilon_{\gamma,m}^{SSC}}\right)^{-\frac{\alpha-3}{2}} & \epsilon_{\gamma,m}^{SSC} < \epsilon_\gamma < \epsilon_{\gamma,c}^{SSC} \quad , \\ \left(\frac{\epsilon_{\gamma,c}^{SSC}}{\epsilon_{\gamma,m}^{SSC}}\right)^{-\frac{\alpha-3}{2}} \left(\frac{\epsilon_\gamma}{\epsilon_{\gamma,c}^{SSC}}\right)^{-\frac{\alpha-2}{2}} & \epsilon_{\gamma,c}^{SSC} < \epsilon_\gamma < \epsilon_{\gamma,max}^{SSC} \quad , \end{cases} \tag{2.38}$$

where $A_{\gamma,SSC}$ is the proportionality constant,

$$A_{\gamma,SSC} = \frac{4\sigma_T}{9} d_z^2 \delta_D^3 U_e \, r_d^3 N_e \gamma_{e,m}^2 \quad . \tag{2.39}$$

Equations 2.38 and 2.39 describe the inverse Compton spectrum as function of the magnetic field B, the electron density N_e, the size of the emission region r_d, the bulk Lorentz factor Γ and the spectral index α. As observed, the inverse Compton spectra is strongly related to the synchrotron spectrum. In fact, the dependency on the parameters is the same for both spectra. A linear correlation between both emission is expected.

For gamma emission in the energy range of hundreds of GeV to TeVs, the main spectral component is the third power law in equation 2.38. For instance, the value for $\epsilon_{\gamma,c}^{SSC}$ is 836.8 GeV for standard values of $r_d = 1.8 \times 10^{16}$ cm, $\Gamma = 22$, $B = 6.1 \times 10^{-2}$ G and $N_{\rm e} = 10^{4.2}\,{\rm cm}^{-3}$. It is not understood what causes a blazar to flare, but if a correlation between gamma-ray emission and X-ray emission is measured, it is interesting to find the parameter space that could reproduce the measured fluxes. For purposes of this thesis, the spectral index is considered fixed and the parameter space is found for different correlations for a blazar similar to Mrk 421.

Chapter 3

Discussion and Conclusions

Blazar exhibits challenges for a leptonic or hadronic model with one-zone emission. These sources demand sometimes atypical parameters for explaining the hard spectrum shape, especially in the TeV gamma-ray band. We propose a one-zone synchrotron self-Compton model to explain the TeV and X-ray observations and its possible correlation during flaring or quiescent states. An electron population with two power-law functions was required to describe these observations. The full set of parameters derived is: Doppler factor, magnetic field, emitting radius and electron density. It is worth noting that although a two emitting region model (more than one electron population) has been proposed for several blazars in order to describe the TeV and X-ray observations, we only require a one emitting zone. Similarly, in our analysis we do not consider accelerated protons in the emitting region, which could require a high intensity of the magnetic field. Although annihilation-line photons may attenuate the TeV gamma-ray spectrum produced in the emitting region, this effect was not analyzed in this thesis. It is relevant to say that our one-zone SSC model was applied to a high peaked synchrotron blazar, and not to a low or intermediate peaked synchrotron blazar, which do not show a lineal correlation as discussed in the literature.

The peak energies of the synchrotron and inverse Compton emissions are at 0.2 keV and 0.8 GeV, respectively. Thus, it makes sense to test the existence of a correlation between fluxes in the energy ranges of tens of keV and hundreds of GeV. One of the most studied blazars at all energies is Mrk 421. In fact, several authors have looked for correlations between TeV γ- and X-ray fluxes during high- and low- activity. For instance, [Macomb, D. J 1995], [Fossati, G. 2008], [Acciari, V. A 2011] and [Aleksić, J. 2015] reported TeV flares in coincidence with flaring activities in X-rays occurred in 1994 May, 2001 March, 2008 May and 2010 March, respectively. They reported strong correlations with no lags. Furthermore, Mrk421 was monitored in γ-rays and X-rays in 2009, between January and June, [Aleksić, J 2015] and in 2013 January - March [Baloković, M. 2016]. In 2009, [Aleksić, J 2015] reported a harder-when-brighter behavior in the X-ray flux, measuring a positive correlation between TeV and X-ray fluxes with zero time lag. In 2013, [Baloković, M. 2016] reported a significant TeV/X-ray correlation on a timescale of about one week. Finally, a robust study in different time scales and flux level of the correlations with a data set for 14 years [Acciari, V. A., 2014] with Whipple was performed by [González, M. M 2019]. The correlation is reproduced by increasing the electron density. They argue that it is possible to describe all flux levels without varying the magnetic field.

In order to test the conclusion, in this thesis we consider a blazar like Mrk 421 and assume different linear correlations. We use our model, described earlier, to reproduce the fluxes within the different hypothetical correlations. This to find the different values of magnetic field and electron density that reproduce the fluxes. To prove the hypothesis. Results are shown in Figure 3.1.

Figure 3.1 shows in lower panels four different correlations, becoming steeper from panel (a) to (d) and, in upper panels, the magnetic field and electron density that reproduce the fluxes in the lower panels. As observed, for a weak correlation, panel (a), the parameter space is broad. As the correlation is steeper, the values of the magnetic field that describes the highest fluxes are narrower. The flaring states are obtained by increasing the electron density. The conclusion by [González, M. M 2019] does not hold for the steepest correlation

when a decrease in the magnetic field is required in order to obtain the highest fluxes. Observations of the polarization may confirm this decrease.

In this thesis, a theoretical model was developed with the minimum number of assumptions such as one electron population described by the simplest function (a broken power law) with a constant spectral index for all levels and duration of activity of the blazar. We do not consider neither hadronic scenarios and its electromagnetic cascades due to photohadronic interactions nor external inverse Compton emission with broadline and dust radiation as seed photons. This allows to perform a model-independent study of the correlation of the VHE γ-ray and the X-ray emission.

For future work, this model could be used to study a sample of high-energy peak BL Lacs, as shown in this thesis. In particular, it is not clear if there is a characteristic magnetic field for each blazar or all blazars will show a correlation between TeV γ- and X-rays. Consequences in the parameter space when a spectral evolution is considered have to be studied. In particular, when the spectrum varies from soft to hard as the flux increases. Here, a theoretical description of the spectrum has been considered, but also a study of the correlation as function of the empirical model fitting the spectra has to be performed. It has been observed a degree of dispersion on the correlation that has to be understood, if it is intrinsic to the blazar, for example, for the existence of more than one electron population or if this is related to systematic in the observations. We want to emphasize that this modeling will be applied to a sample of high-energy peak BL Lacs.

Further studies in the dependencies of the parameters analyzed need to be done to understand better the acceleration mechanisms, radiation processes and jet composition, among others in blazars.

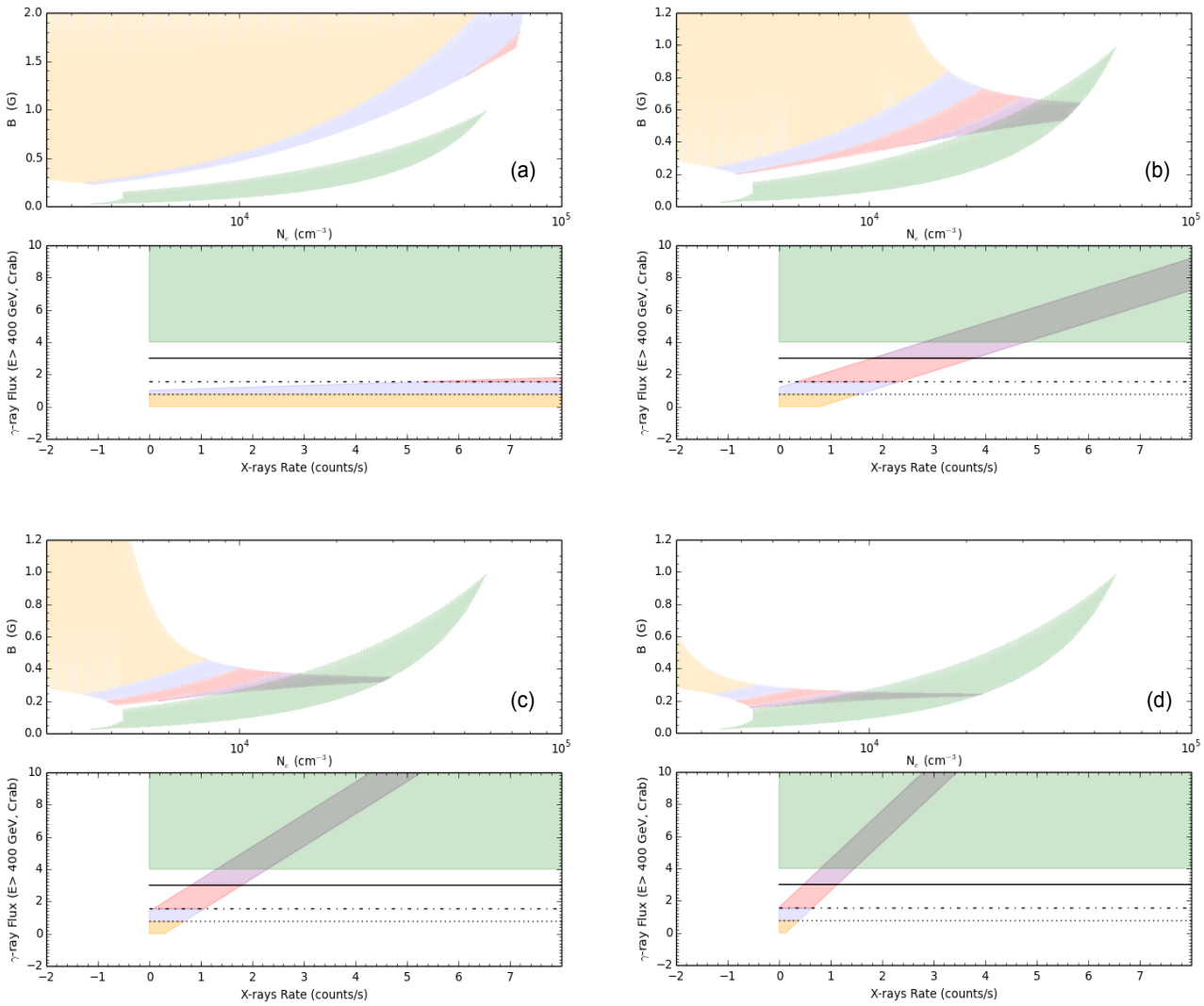

Figure 3.1: Theoretical Results.

Panel (a): 2D parameter space (upper) allowed by hypothetical correlation of emission in VHE γ-rays and X-rays for a source as Mrk 421 (lower). The 2D parameter space corresponds to the magnetic field and electron density, and the hypothetical correlation are for a slope of 0.10 ± 0.02. The regions in yellow, purple, pink and violet represent levels of flux activity of the source within the correlation, from the very-low, low, high and very-high states, respectively. The green region corresponds to highest gamma ray fluxes observed for Mrk 421, some of them not following the correlation and associated to orphan flares. The "very low", "low" and "high" states of Mrk 421, as measured by VERITAS, are displayed as black dotted, dot-dashed and solid lines, respectively. Panel (b), (c) and (d) are the same as panel (a) but the hypothetical correlations with slopes of 1.0 ± 0.2, 2.0 ± 0.4 and 3.0 ± 0.6.

Chapter 4

Appendix A

4.1 Emission and Absorption Lines

An emission line appears in a spectrum, if the source emits specific wavelength of radiation. An emission takes place when electrons in an atom, which are excited (e.g. being heated,...), make a transition from a high energy state to a lower energy state. When the electron falls back and leave the excited state, the energy is re-emitted in the form of a photon. [COSMOS, Osterbrock, D. 2006]

An absorption line appears in a spectrum, if an absorbing material is located between the source and the observer. Such material may be outer layers of a star, a cloud of interstellar gas or a cloud of dust. An atom, atomic nuclei or molecule may absorb photons with a given energy if such energy is equal to the difference between two of their energy states. This lines are seen usually as dark lines or lines of reduced intensity. [COSMOS, Osterbrock, D. 2006]

4.2 Broad and Narrow Lines

The broad lines of AGNs come from material close to the BH, they are broadened because the emitting material is revolving around the BH with high velocities causing Doppler shifts of the emitted radiation. The narrow lines come from an emitting region farther from the BH, moving slower, which causes the, to narrower than the broad lines. [Osterbrock, D. 2006]

Chapter 5

Appendix B: Physics background

5.1 Synchrotron Radiation

Synchrotron radiation may be defined as the radiation emitted by charged relativistic particles in interaction with a magnetic field. The following discussion is based on the concepts presented in Rybicki's *Radiative Processes in Astrophysics* textbook [Rybicki, G. 1986].

5.1.1 Power Emitted

So as mentioned before, and in a bold manner, we may say synchrotron radiation is due to a charged particle moving at relativistic velocities in interaction with a magnetic field, which proceeds to move in a helical motion, as shown in figure 5.1. Keeping this in mind, we will start by finding the motion of a particle of mass, m, and charge, q, in a magnetic field, to proceed on calculating the magnetic field at hand and, therefore, be able to find our total power emitted, this to allow us to understand the processes it takes for this radiation to be

emitted and the energy that it conveys. Perhaps, to do so, we will first study the case of one particle opposed to the distribution of charged particles known to participate in this process, this for a better understanding. Taking in consideration all the above mentioned, when we speak of finding the equation of motion of a particle, we imply the forces that act upon this particle, in this case, we have the Lorentz force acting upon it due to the magnetic field (we will use Lorentz four-force notation as seen on equation 5.1).

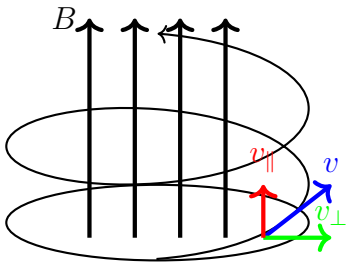

Figure 5.1: Helical motion of a particle in an uniform magnetic field.

$$F^{\nu} = \frac{q}{c} F^{\nu}_{\mu} U^{\mu}. \tag{5.1}$$

Where q is the charge of the particle, c is the speed of light and $(F_{\nu\mu})$ Maxwell's tensor, which represents the interaction between electromagnetic forces and mechanical momentum, is given by

$$F_{\nu\mu} = \begin{pmatrix} 0 & -E_x & -E_y & -E_z \\ E_x & 0 & B_z & -B_y \\ E_y & -B_z & 0 & B_x \\ E_z & B_y & -B_x & 0 \end{pmatrix},$$

where E_i are the components of the electric field, B_i are the components of the magnetic field and ν and μ are the subscript and upperscript of the tensor and the four-velocity vector is

$$U^{\mu} = \begin{pmatrix} c \\ v_x \\ v_y \\ v_z \end{pmatrix}.$$

Using the above mentioned, we find that

$$\frac{d}{dt}(\gamma m\vec{v}) = \frac{q}{c}\vec{v}\times\vec{B}, \tag{5.2}$$

$$\frac{d}{dt}(\gamma mc^2) = q\vec{v}\cdot\vec{E} = 0. \tag{5.3}$$

As shown in figure 5.1, when a charged particle enters into an uniform magnetic field it has a helical motion where the Lorentz force acting upon the particle acts as a centripetal force, making the particle go in circles, changing the velocity's direction, but not its magnitude. The combination of this circular motion and the uniform motion along the field is a helical motion of the particle. This change is perpendicular to the magnetic field. Separating the velocity components along the field, we have the following

$$\frac{d}{dt}v_{\parallel} = 0,$$

$$\frac{d}{dt}v_{\perp} = \frac{q}{\gamma mc}v_{\perp}B\sin\alpha_s.$$

Where α_s is the angle between v and B. The frequency of the rotation, or gyration is

$$\omega_B = \frac{qB}{\gamma mc}. \tag{5.4}$$

Finding the equation of motion allowed us to find the acceleration of the particle and, in turn, its gyration, which will be needed in the following derivations.

Now to, find total power emitted, we are going to consider the retarded potentials (the Liénard-Wiechart potentials). We are going to find the magnetic field, which in turn, will lead as to the derivation of the power emitted. Considering a particle of charge, q, that moves along a trajectory, $\vec{r} = r_0(t)$, and its velocity at any time is $\vec{v}(t) = \dot{r}_0(t)$. The charge and current densities are given by

$$\rho(\vec{r'},t) = q\delta^3(\vec{r'} - \vec{r}_0(t_{ret})),$$

$$\vec{j}(\vec{r'},t) = q\vec{v}(t)\delta^3(\vec{r} - \vec{r}_0(t_{ret})).$$

We need the charge density at a retarded time, to which we can write as the integral over time of the charge density multiplied, by another delta function

$$\rho(\vec{r},t) = q\delta^3(\vec{r'} - \vec{r}_0(t')) \int dt' \delta(t' - t_{ret}).$$

To find the scalar potential, we have

$$\phi = \int \frac{d^3\vec{r'}\delta^3(\vec{r'} - \vec{r}_0(t_{ret})}{|\vec{r} - \vec{r'}|} \int dt' \delta\left(t' - \left(t - \frac{\vec{r} - \vec{r'}}{c}\right)\right),$$

doing the spatial integration, the delta function is nonzero only where its argument is zero, so all contributions to the integral come where $\vec{r'} = r_0(t')$. With $\mathbf{R}(t') = \vec{r} - \vec{r}_0(t')$ and $R = |\mathbf{R}(t')|$. We then have

$$\begin{aligned} \phi &= q \int R^{-1}(t')\delta(t' - t + R(t')/c)dt', \\ A &= \frac{q}{c} \int \vec{v}(t')R^{-1}(t')\delta(t' - t + R(t')/c)dt'. \end{aligned}$$

Delta function vanishes for $t' = t_{ret}$. Let us change variables $t'' = t'$, so we have $dt'' = dt' + \frac{1}{c}\dot{R}(t')dt' = (1 + \frac{1}{c}\dot{R}(t'))dt'$ also we will define the unit vector, $\eta = \frac{\mathbf{R}}{R}$, and we have $\dot{R}(t') = -\eta\vec{v}(t')$. So, the potentials in terms of η and t'' allow us to easily solve the integrals with the delta function setting in $t'' = 0 \equiv t_{ret}$. So, we obtain the Liénard-Wiechart potentials, where the brackets denote retarded times.

$$\phi = \left[\frac{q}{\kappa R}\right], \tag{5.5}$$

$$A = \left[\frac{q\vec{v}}{c\kappa R}\right]. \tag{5.6}$$

Using the above, we solve for $|\vec{E}_{rad}| = |\vec{B}_{rad}| = \frac{q\dot{\vec{v}}}{Rc^2}\sin\Theta$ and the Poynting vector is in the direction of η and has a magnitude

$$S = \frac{c}{4\pi}E_{rad}^2 = \frac{c}{4\pi}\frac{q^2\dot{\vec{v}}^2}{R^2c^4}\sin^2\Theta. \tag{5.7}$$

This corresponds to an outward flow of energy, along the direction $\vec{\eta}$. We can put this into the form of an emission coefficient. The energy $d\vec{W}$ emitted per unit time into solid angle $d\Omega$ about $\vec{\eta}$ can be evaluated by multiplying the Poynting vector by the area $dA = R^2 d\Omega$ represented by Ω at the field point:

$$\frac{d\vec{W}}{dtd\Omega} = \frac{q^2\dot{\vec{v}}^2}{4\pi c^3}\sin^2\Theta. \tag{5.8}$$

We may obtain the total power emitted into all angles by integrating this over the solid angle:

$$P = \frac{d\vec{W}}{dt} = \frac{q^2\dot{\vec{v}}^2}{4\pi c^3}\int \sin^2\Theta d\Omega. \tag{5.9}$$

So we obtain the Larmor's formula

$$P = \frac{2q^2\dot{\vec{v}}^2}{3c^3} = \frac{2q^2\vec{a}^2}{3c^3}. \tag{5.10}$$

Expressing P in terms of the three-vector acceleration

$$P = \frac{2q^2}{3c^3}\gamma^4(a_\perp^2 + \gamma^2 a_\parallel^2). \tag{5.11}$$

The acceleration is perpendicular to the velocity, with magnitude $a_\perp = \omega_B v_\perp$, so that the total emitted radiation is,

$$P = \frac{2q^2}{3c^3}\gamma^4\frac{q^2B^2}{\gamma^2 m^2 c^2}v_\perp^2. \tag{5.12}$$

For an isotropic distribution of velocities, it is necessary to average this formula over all angles for a given speed β. Let α be the pitch angle, which is the angle between the field and the velocity. Then we obtain

$$\langle\beta\rangle = \frac{\beta^2}{4\pi}\int \sin^2\alpha d\Omega = \frac{2\beta^2}{3}. \tag{5.13}$$

The total power emitted can also be written in terms $\sigma_T = 8\pi r_0^2/3$, which is the Thomson cross section, $U_B = B^2/8\pi$ is the magnetic energy density and the classical electron radius $r_0 = q^2/mc^2$.

$$P = \frac{4}{3}\sigma_T c\beta^2\gamma^2 U_B. \tag{5.14}$$

5.1.2 Spectrum

Now that we have the total power emitted, we will discuss the spectrum of synchrotron radiation, which must be related to the detailed variation of the electric field as seen by the observer. Due to beaming effects, the emitted fields appear to be concentrated in a narrow

set of directions about the particle's velocity. The observer will see a pulse of radiation confined to a time interval much smaller than the gyration period. The spectrum will be spread over a much broader region than one of order $\omega_B/2\pi$.

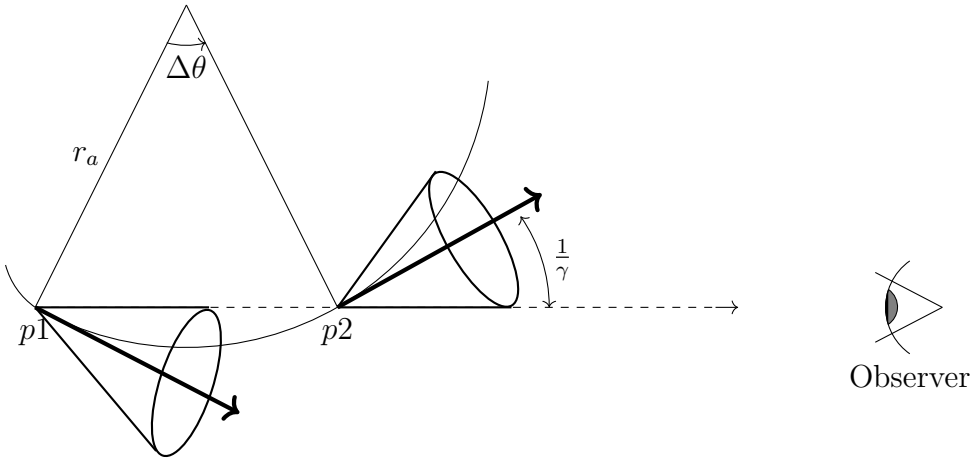

Figure 5.2: Emission cones at different points of an accelerated particle's trajectory.

In figure 5.2, we can tell that the observer will see the pulse from points p_1 and p_2 along the particle's path, where these points are such that the cone of emission of angular width $\sim 1/\gamma$ includes the direction of observation. The distance Δs, along the path, can be computed from the radius of curvature of the path, $r_a = \Delta s/\Delta\theta$, and from geometry, we know $\Delta\theta = 2/\gamma$, so that $\Delta s = 2r_a/\gamma$. Using the equation of motion we found earlier, since $|\Delta\vec{v}| = v\Delta\theta$ and $\Delta = v\Delta t$, we may rewrite the equation is terms of the radius of curvature of the path and the gyration as

$$r_a = \frac{v}{\omega_B \sin\alpha}. \tag{5.15}$$

In turn, Δs is given by

$$\Delta s \approx \frac{2v}{\gamma\omega_B \sin\alpha}. \tag{5.16}$$

The time t_{p1} and t_{p2} (time at which the particle passes through point p_1 and p_2 respectively) are given by $\Delta s = v(t_{p2} - t_{p1})$, so that

$$\Delta t_{em} = t_{p2} - t_{p1} \approx \frac{2}{\gamma\omega_B \sin\alpha}. \tag{5.17}$$

This duration of emission (or emission time) is given by the arclength traversed given a gyration radius r_a, combined with the velocity v, of the particle while the time it takes the

radiation to move a distance Δs (the time it takes the light to travel from the beginning and the end of the emission), we will call it traveled time and is given by $\Delta t_{trav} = \Delta s/c = 2v/\gamma c\omega_B \sin\alpha$. The arrival time is the difference of the time of the emission and the time it takes for it to travel from the beginning and the end of the emission. So the traveled time is given by

$$\Delta t_A = \frac{2}{\gamma\omega_B \sin\alpha}\left(1 - \frac{v}{c}\right) \approx \frac{1}{\gamma^3\omega_B \sin\alpha}. \tag{5.18}$$

We expect that the spectrum will be fairly broad, cutting off at frequencies like $1/\Delta t_A$, defining a critical frequency, which is where we have the maximum power emitted in the spectrum, then we expect the spectrum to extend to something of order ω_c before falling away, where ω_c follows

$$\omega_c \equiv \frac{3}{2}\gamma^3\omega_B \sin\alpha. \tag{5.19}$$

or

$$\nu_c = \frac{3}{4\pi}\gamma^3\omega_B \sin\alpha. \tag{5.20}$$

We can obtain a lot of information about the spectrum, by using the fact that the electric field is a function of θ just through the combination $\gamma\theta$, where θ is a polar angle about the direction of motion. So we have $E(t) \propto F(\gamma\theta)$, where t is the time measured in the observer's frame. We set the zero of time and the path length s to be when the pulse is centered on the observer. Using arguments similar to those used to find Δs, we find $\theta \approx s/a$ and $t \approx (s/v)(l - v/c)$. Then, the relationship of θ to t is found to be $\gamma\theta \approx 2\gamma(\gamma^2\omega_B \sin\alpha)t \propto \omega_c t$. This way, we can derive the dependence of the spectrum on ω. The Fourier transform of the electric field is $\hat{E}(\omega)\int_{-\infty}^{\infty} g(\omega_c t)e^{i\omega t}dt$. The spectrum $dW/d\omega$ is proportional to the square of $\hat{E}(\omega)$. Integrating this over solid angle and dividing by the orbital period, both independent of frequency, gives the time averaged power per unit frequency, $dW/dtd\omega = T^{-1}dW/d\omega \equiv P(\omega) = C_1F(\omega/\omega_c)$ where F is a dimensionless function and C_1 is a constant of proportionality. In turn, we have

$$P = \frac{2q^4B^2\gamma^2\beta^2\sin^2\alpha}{3m^2c^3}. \tag{5.21}$$

and

$$\omega_c = \frac{3\gamma^2 qB\sin\alpha}{2mc} \tag{5.22}$$

We find that, for the highly relativistic case ($\beta \approx 1$), the power per unit frequency emitted by each electron is

$$P(\omega) = \frac{\sqrt{3}}{2\pi} \frac{q^3 B \sin\alpha}{mc^2} F\left(\frac{\omega}{\omega_c}\right). \tag{5.23}$$

In formula for $P(\omega)$ given above, we can easily tell there is no factor of γ appears, except for that contained in ω_c. This fact is enough to derive an extremely important result concerning synchrotron spectra. Often, the spectrum can be approximated by a power law over a limited range of frequencies. When this is so, we may define the spectral index as the constant α in the following expression

$$P(\omega) \propto \omega^{-\alpha}. \tag{5.24}$$

This is the negative slope on a $\log - \log$ plot. Usually, the spectra of astronomical radiation has a spectral index that is constant over a fairly wide range of frequencies: for example, the Rayleigh-Jeans portion of the blackbody law has $\alpha = -2$. A similar result sometimes holds for the particle distribution law of relativistic electrons. Often, the number density of particles with energies between E and $E + dE$ (or γ and $\gamma + d\gamma$) can be approximately expressed in the form

$$N(E)dE = CE^{-p}dE. \tag{5.25}$$

or

$$N(\gamma)d\gamma = C\gamma^{-p}d\gamma \tag{5.26}$$

The total power radiated per unit volume per unit frequency by such a distribution is given by the integral of $N(\gamma)d\gamma$ times the single particle radiation formula over all energies or γ.

$$P(\omega) = C\int_{\gamma_1}^{\gamma_2} P(\omega)\gamma^{-p}d\gamma \propto \int_{\gamma_1}^{\gamma_2} F\left(\frac{\omega}{\omega_c}\right)\gamma^{-p}d\gamma \tag{5.27}$$

Integrating, we find that our spectral index is given by

$$\alpha = \frac{p-1}{2} \tag{5.28}$$

5.2 Inverse Compton

The following discussion, just as the previous section is based on knowledge acquired from Rybicki's *Radiative Processes in Astrophysics* textbook [Rybicki, G. 1986].

5.2.1 Energy Transfer

First, we are going to discuss some previous concepts to understand Inverse Compton scattering, starting with the scattering from electrons at rest. For low photon energies, $h\nu \ll m_e c^2$, the scattering of radiation from free charges process is Thomson scattering which describes photon scattering by free electrons in the low energy limit, the incident photons are approximated as a continuous electromagnetic wave. We assume an electron at rest, and an electromagnetic wave of frequency $\nu \ll m_e c^2/h$, also that the incoming wave is completely linearly polarized. In order to neglect the magnetic force $(q/c)(\vec{v} \times \vec{B})$, we require that the oscillation velocity to be $v \ll c$. This, in turn, implies that the incoming wave has a sufficiently low amplitude. The electron starts to oscillate ($\vec{E} = E_0 \sin \omega t \hat{z}$) in response to the varying electric force qE ($m_e \frac{d^2 z}{dt} = q_e E_0 \sin \omega t = m_e a$), and the average square acceleration ($\langle a \rangle = \sqrt{a^2}$) is

$$\langle a^2 \rangle = \frac{e^2 E_0^2}{2m^2}. \tag{5.29}$$

The emitted power per unit solid angle is given by the Larmor formula $dP/d\Omega = q^2 a^2 \sin^2 \Theta/(4\pi c^3)$ (equation 5.9, before integrating over the solid angle), where Θ is the angle between the acceleration vector and the propagation vector of the emitted radiation. Note that Θ is not the scattering angle, which is the angle between the incoming and the scattered wave (or photon). We have

$$\frac{dP}{d\Omega} = \frac{q^2 E_0^2}{8\pi m^2 c^3} \sin^2 \Theta. \tag{5.30}$$

The scattered radiation is completely linearly polarized in the plane defined by the

incident polarization vector and the scattering direction. The flux of the incoming wave is $\frac{dP}{d\sigma} = S_i = cE_0^2/(8\pi)$. The differential cross section of the process is then

$$\frac{d\sigma}{d\Omega} = \frac{dP/d\Omega}{S_i} = r_0^2 \sin^2 \Theta. \tag{5.31}$$

The total cross section can be derived in a similar way, but considering the Larmor formula integrated over the solid angle (equation 5.10). The total cross section is

$$\sigma_T = \frac{P}{S_i} = \frac{8\pi}{3} r_0^2. \tag{5.32}$$

To find the scattering of an unpolarized incoming wave, we will assume that the incoming radiation is the sum of two orthogonal completely linearly polarized waves, and then adding the associated scattering patterns. Since we have the freedom to chose the orientations of the two polarization planes, it is convenient to chose one of these planes as the one defined by the incident and scattered directions, and the other one perpendicular to this plane. The scattering can be then considered as the sum of two independent scattering processes, one with emission angle Θ, the other with $\pi/2$. The scattering angle (the angle between the scattered wave and the incident wave) is $\theta = \pi/2 - \Theta$, we have

$$\frac{d\sigma_T}{d\Omega} = \frac{1}{2} r_0^2 (1 + \cos^2 \theta). \tag{5.33}$$

We have ϵ and ϵ_1 are the incident and scattered photon energy, respectively, $d\sigma_T/d\Omega$ is the differential Thomson cross section for unpolarized incident radiation, and r_0 is the classical electron radius, when $\epsilon = \epsilon_1$ the scattering is called elastic. Here, we have review Thomson scattering, including Thomson cross section, now we will proceed to find the energy of a scattered photon. We assumed that the electron is at rest, the initial and final four-momenta of the photon are $\vec{P}_{\gamma i} = (\epsilon/c)(1, n_i)$ and $\vec{P}_{\gamma f} = (\epsilon_1/c)(1, n_f)$, and the initial and final momenta of the electron are $P_{ei} = (mc, 0)$ and $P_{ef} = (E/c, p)$,where n_i and n_f are the initial and final directions of the photons as shown in figure 5.3. Conservation of momentum and energy is expressed by $\vec{P}_{ei} + \vec{P}_{\gamma i} = \vec{P}_{ef} + \vec{P}_{\gamma f}$. Rearranging terms and squaring gives $|\vec{P}_{ef}|^2 = |\vec{P}_{ei} + \vec{P}_{\gamma i} - P_{\gamma f}|^2$ which eliminates the final electron momentum. We obtain

$$\epsilon_1 = \frac{\epsilon}{1 + \frac{\epsilon}{mc^2}(1 - \cos\theta)}. \tag{5.34}$$

In terms of wavelength, this can be written as

$$\lambda_1 - \lambda = \lambda_c(1 - \cos\theta), \tag{5.35}$$

where the Compton wavelength is defined by

$$\lambda_c = \frac{h}{mc}. \tag{5.36}$$

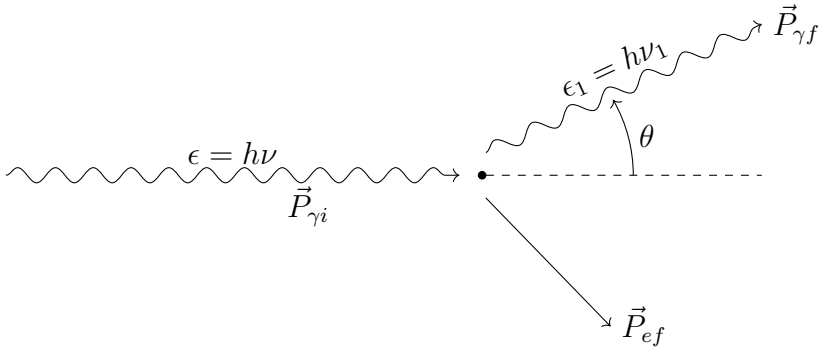

Figure 5.3: Geometry of the scattering of a photon by an electron initially at rest.

We found that change of the wavelength is of the order of λ_c, upon scattering. For long wavelengths, $\lambda \gg \lambda_c$ ($hv \ll mc^2$), the scattering is closely elastic. When this condition is met, we can assume that there is no change in the photon energy in the rest frame of the electron. The differential cross section for unpolarized radiation is shown in quantum electrodynamics (Heitler, 1954) to be given by the Klein-Nishina formula

$$\frac{d\sigma}{d\Omega} = \frac{r_0^2}{2}\frac{\epsilon_1^2}{\epsilon^2}\left(\frac{\epsilon}{\epsilon_1} + \frac{\epsilon_1}{\epsilon} - \sin^2\theta\right). \tag{5.37}$$

In the non relativistic regime, we have approximately($x \ll 1$)

$$\sigma \approx \sigma_T\left(1 - 2x + \frac{26x^2}{5} + ...\right), \tag{5.38}$$

for the extreme relativistic regime we have ($x \gg 1$)

$$\sigma = \frac{3}{8}\sigma_T x^{-1}\left(\ln 2x + \frac{1}{2}\right), \tag{5.39}$$

where $x \equiv h\nu/mc^2$.

When the electron is not at rest, but has an energy greater that the typical photon energy, there can be a transfer of energy from the electron to the photon. This process is called inverse Compton. Let us call K the lab or observer's frame, and let K' be the rest frame of the electron. Note that the previous expressions for scattering of electrons at rest should now be primed. The scattering event as seen in each frame is given in figure 5.4

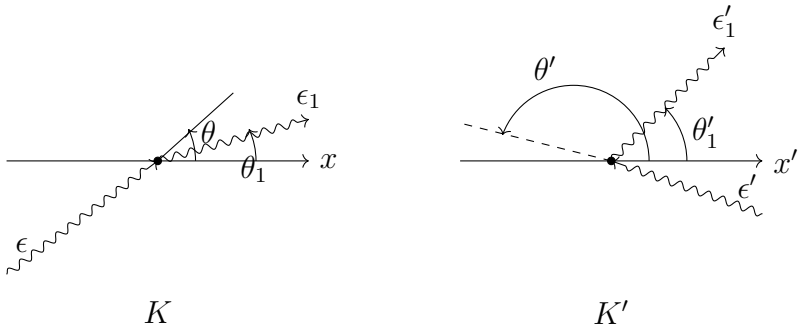

Figure 5.4: Scattering geometries in the observer's frame K and in the electron rest frame K'.

So we obtain the incident and scattered photon energy

$$\epsilon' = \epsilon\gamma(1 - \beta\cos\theta), \tag{5.40}$$

$$\epsilon_1 = \epsilon_1'\gamma(1 + \beta\cos\theta_1'). \tag{5.41}$$

We also know

$$\epsilon_1' \approx \epsilon' \left(1 - \frac{\epsilon'}{mc^2}(1 - \cos\Theta)\right), \tag{5.42}$$

$$\cos\Theta = \cos\theta_1'\cos\theta' + \sin\theta'\sin\theta_1'\cos(\phi' - \phi_1'), \tag{5.43}$$

where ϕ_1' and $\phi'$are the azimuthal angles of the scattered photon and incident photon in the rest frame. In the case of relativistic electrons, $\gamma^2 - 1 \gg h\nu/mc^2$, the energies of the photon before scattering, in the rest frame of the electron, and after scattering are in the approximate ratios

$$1 : \gamma : \gamma^2 \tag{5.44}$$

providing that the condition for Thomson scattering in the rest frame $\gamma\epsilon \ll mc^2$ is met. This process, therefore, turns a low-energy photon to a high-energy one by a factor of order

γ^2. Since the intermediate photon energy can be as high, perhaps up to 100 keV, and still be in the Thomson limit, it can be seen that photons of high energies ($\gamma \times 100keV$) can be produced. From the conservation of energy, we can write $\epsilon_1' < \gamma mc^2 + \epsilon$. Fixing ϵ and letting γ become large, we see that photon energies larger than $\sim \gamma mc^2$ cannot be obtained. So, we found the energy transmitted from an electron at rest and from electrons in motion.

5.2.2 IC Power Emitted

Now, we want to find the formulas for the case of a given isotropic distribution of photons scattering off a given isotropic distribution of electrons. Here, we have the photon phase space distribution function ($n(p)$), which is a Lorentz invariant and $vd\epsilon$ is the density of photons having energy in range $d\epsilon$. Then v and n are related by

$$vd\epsilon = nd^3p, \tag{5.45}$$

in turn

$$\frac{vd\epsilon}{\epsilon} = \frac{v'd\epsilon'}{\epsilon'}. \tag{5.46}$$

The total power emitted (scattered) in the electron's rest frame can be found from

$$\frac{dE_1'}{dt'} = c\sigma_T \int \epsilon_1' v' d\epsilon', \tag{5.47}$$

where $v'd\epsilon'$ is the number density of incident photons. Now we will assume that the change in energy of the photon in the rest frame is negligible compared to the energy change in the lab frame, $\gamma^2 - 1 >> \epsilon/mc^2$; thus we can equate $\epsilon_1' = \epsilon'$. Now,

$$\frac{dE_1}{dt} = \frac{dE_1'}{dt}, \tag{5.48}$$

by the invariance of emitted power. So, using Lorentz invariants we have

$$\frac{dE_1}{dt} = c\sigma_T \int \epsilon'^2 \frac{v'd\epsilon'}{\epsilon'} = c\sigma_T \int \epsilon'^2 \frac{vd\epsilon}{\epsilon}. \tag{5.49}$$

Here we assumed that $\gamma\epsilon \ll mc^2$, so that the Thomson cross section is applicable. Considering equation 5.40, we can say

$$\frac{dE_1}{dt} = c\sigma_T\gamma \int (1 - \beta\cos\theta)\epsilon v d\epsilon, \tag{5.50}$$

this in the K frame. Considering an isotropic distribution of photons we have

$$\frac{dE_1}{dt} = c\sigma_T\gamma^2\left(1+\frac{1}{3}\beta^2\right)U_{ph}, \tag{5.51}$$

where

$$U_{ph} \equiv \int \epsilon v d\epsilon, \tag{5.52}$$

which is the initial photon energy density. The rate of decrease of the total initial photon energy is

$$\frac{dE_1}{dt} = -c\sigma_T \int \epsilon v d\epsilon = -\sigma_T c U_{ph}. \tag{5.53}$$

Therefore, the net power lost by the electron, and, thereby, converted into increased radiation is

$$\frac{dE_{rad}}{dt} = c\sigma_T U_{ph}\left[\gamma^2\left(1+\frac{1}{3}\beta^2\right)-1\right]. \tag{5.54}$$

So we find that the power is

$$P_{comp} = \frac{dE_{rad}}{dt} = \frac{4}{3}\sigma_T c\gamma^2\beta^2 U_{ph}. \tag{5.55}$$

When the energy transfer in the electron rest frame is not neglected, equation 5.55 becomes

$$P_{comp} = \frac{dE_{rad}}{dt} = \frac{4}{3}\sigma_T c\gamma^2\beta^2 U_{ph}\left[1-\frac{63}{10}\frac{\gamma\langle\epsilon^2\rangle}{mc^2\langle\epsilon\rangle}\right], \tag{5.56}$$

where $\langle\epsilon^2\rangle$ and $\langle\epsilon\rangle$ are the mean values integrated over U_{ph}. Note that equation 5.56 allows energy to be either given or taken from the photons. From our discussion on synchrotron radiation, we found that the power emitted by each electron is given by equation 5.14. Using this, we find

$$\frac{P_{synch}}{P_{comp}} = \frac{U_B}{U_{ph}}, \tag{5.57}$$

the radiation losses due to synchrotron emission and to inverse Compton effect are in the same ratio as the magnetic field energy density and photon energy density. Note that this result also remains true for arbitrary values of the electron's velocity, not just for ultra relativistic values. It does, however, depend on the validity of Thomson scattering in the rest frame so that $\gamma\epsilon \ll mc^2$.

Let $N(\gamma)d\gamma$ be the number of electrons per unit volume with γ in the range γ to $\gamma + d\gamma$. So then, the total power emitted is of the form of

$$P_{tot} = \int P_{comp} N(\gamma) d\gamma, \tag{5.58}$$

if we consider

$$N_e(\gamma_e) = \begin{cases} C\gamma^{-P} & \gamma_{min} < \gamma < \gamma_{max} \\ 0 & otherwise, \end{cases} \tag{5.59}$$

then, with $\beta \sim 1$ we have

$$P_{tot} = \frac{4}{3}\sigma_T U_{ph} C (3-p)^{-1} \left(\gamma_{max}^{3-p} - \gamma_{min}^{3-p}\right). \tag{5.60}$$

If we, instead, find the total power from a thermal distribution of nonrelativistic electrons of number density n_e and let $\gamma \approx 1$ and $\langle \beta^2 \rangle = 3kT/mc^2$ we have

$$P_{tot} = \frac{4kT}{mc^2} c\sigma_T n_e U_{ph}, \tag{5.61}$$

where $\frac{4kT}{mc^2}$ is the fractional photon energy gain per scattering when $\epsilon \ll 4kT$.

5.2.3 IC Spectrum

Now that we found the total power emitted, let's discuss its spectrum, which here it depends on both the incident spectrum and the energy distribution of the electrons. Though this is true we can only determine the spectrum for the scattering of photons of a given energy ϵ_0 off electrons of a given energy γmc^2, since the general spectrum can be found by averaging over the actual distribution of photons and electrons. We will consider isotropic distributions for both the electrons and photons, therefore, the scattered photons are then also isotropically distributed, so we will just need to find their energy spectrum.

Here, we will consider that the scattering in the rest frame is isotropic we assume that $\frac{d\sigma'}{d\Omega} = \frac{1}{4\pi}\sigma_T = \frac{2}{3}r_0^2$, also it is convenient to refer to intensity, I, based on the photon number

rather than energy. The number of photons crossing area dA in time dt within solid angle $d\Omega$ and energy range $d\epsilon$, $IdAdtd\Omega d\epsilon$. This intensity can be found from the monochromatic specific intensity by dividing by the energy. Suppose that the isotropic incident photon field is monoenergetic, $I(\epsilon) = F_0\delta(\epsilon - \epsilon_0)$ where F_0 is the number of photons per unit area, per unit time per steradian. So, now we will determine the scattering of a beam of electrons of density N and energy γmc^2 traveling along the x axis (as shown in figure 5.4). The incident intensity field in the rest frame K' is

$$I'(\epsilon', \mu') = F_0 \left(\frac{\epsilon'}{\epsilon}\right)^2 \delta(\epsilon - \epsilon_0). \tag{5.62}$$

We find that the number of emitted photons per unit volume per unit steradian, for elastic scattering (assuming ϵ the incident energy equals ϵ_1' the scattered photon energy), So it follows

$$j'(\epsilon_1') = \begin{cases} \frac{N'\sigma_T\epsilon_1' F_0}{2\epsilon_0^2\gamma\beta} & \frac{\epsilon_0}{\gamma(1+\beta)} < \epsilon_1' < \frac{\epsilon_0}{\gamma(1-\beta)} \\ 0 & otherwise, \end{cases} \tag{5.63}$$

The emission function in frame K can be found from Lorentz invariant $\frac{j_\nu}{\nu^2}$,

$$j(\epsilon_1, \mu_1) = \begin{cases} \frac{\epsilon_1}{\epsilon_1'} j'(\epsilon_1'), & \\ \frac{N\sigma_T\epsilon_1 F_0}{2\epsilon_0^2\gamma^2\beta} & \frac{\epsilon_0}{\gamma^2(1+\beta)(1-\beta\mu_1)} < \epsilon_1 < \frac{\epsilon_0}{\gamma(1-\beta)(1-\beta\mu_1)}, \\ 0 & otherwise. \end{cases} \tag{5.64}$$

The above results hold for a beam of electrons. To obtain the results for an isotropic distribution of electrons, we shall average over the angle between the electron and emitted photon we obtain

$$j(\epsilon_1) = \frac{N\sigma_T F_0}{4\epsilon_0^2\gamma^2\beta^2} \begin{cases} (1+\beta)\frac{\epsilon_1}{\epsilon_0} - (1-\beta) & \frac{1-\beta}{1+\beta} < \frac{\epsilon_1}{\epsilon_0} < 1 \\ (1+\beta) - \frac{\epsilon_1}{\epsilon_0}(1-\beta) & 1 < \frac{\epsilon_1}{\epsilon_0} < \frac{1+\beta}{1-\beta} \\ 0 & otherwise, \end{cases} \tag{5.65}$$

We can easily check that

$$\begin{aligned} \int_0^\infty j(\epsilon_1)d\epsilon_1 &= N\sigma_T F_0, \\ \int_0^\infty j(\epsilon_1)(\epsilon_1 - \epsilon_0)d\epsilon_1 &= N\sigma_T \frac{4}{3}\gamma^2\beta^2\epsilon_0 F_0. \end{aligned}$$

Since $N\sigma_T F_o$ is the rate of photon scattering per unit volume, per unit solid angle, the first of these shows the conservation of number of photons upon scattering. The second shows the average increase in photon energy per scattering.

The spectrum resulting from the scattering of an arbitrary initial spectrum with a power law distribution (as in equation 5.59) of relativistic electrons can now be found, we will use $v(\epsilon)$, the initial photon number density (from equation 5.45) which is related to the isotropic intensity by $v(\epsilon) = 4\pi c^{-1} I(\epsilon)$. The total scattered power per volume per energy is

$$\frac{dE}{dV dt d\epsilon_1} = 4\pi\epsilon_1 j(\epsilon_1) = \frac{3}{4} c\sigma_T C \int d\epsilon \left(\frac{\epsilon_1}{\epsilon}\right) v(\epsilon) \int_{\gamma_1}^{\gamma_2} d\gamma \gamma^{-p-2} f\left(\frac{\epsilon}{4\gamma^2\epsilon}\right). \tag{5.66}$$

The spectral index that we find is

$$\alpha = \frac{p-1}{2}, \tag{5.67}$$

just as the one found for synchrotron emission.

Acknowledgements

This research was financially supported by ***Programa de Apoyo a Proyectos de Investigación e Innovación Tecnológica (PAPIIT) AG-100317, IN106521 and IG101320***.

Bibliography

[Padovani, P. 2017] Padovani, P.; Alexander, D.M.; Assef, R.J.
Active galactic nuclei: what's in a name?, The Astronomy and Astrophysics Review, 2017, 25, 2. DOI

[Malizia, A. 2020] Malizia, A. ; Sazonov, S.; Bassani, L.; Pian, E.; Beckmann, V.; Molina, M.; Mereminskiy, I.; Belanger, G.
INTEGRAL view of AGN, New Astronomy Reviews, Volume 90, article id. 101545, 2020. DOI

[Urry, M.; Padovani, P. 1995] Urry, M.; Padovani, P.
Unified Schemes for Radio-Loud Active Galactic Nuclei,Publications of the Astronomical Society of the Pacific, 1995, v.107, p.803,DOI

[Böttcher, M. 2013] Böttcher, M.; Reimer, A.; Sweeney, K.; Prakash, A.
Leptonic and Hadronic modeling of Fermi-Dectected Blazars, 2013, ApJ, 768, 54, DOI

[Netzer, H. 2013] Netzer, Hagai
The physics and evolution of active galactic nuclei textbook, Cambridge University Press DOI

[Tavecchio, F. 1998] Tavecchio, F.; Maraschi, L.; Ghisellini, G.
Contstraints on the physical parameters of TeV blazars, 1998, ApJ, 509, 608-619, DOI

[González, M. M 2019] González, M. M.; Patricelli, B; Fraija, N.; García-González, J.
Reconcilement of VHE γ-ray/X-ray correlation studies in Mrk 421 and break-down at high fluxes, 2019, MNRAS, 484, 2944, DOI

[Macomb, D. J 1995] Macomb, D. J; Akerlof, C. W.; Aller, H. D;...
Multiwavelength Observations of Markarian 421 During a TeV/X-Ray Flare, 1995, Astrophysical Journal Letters , 449, L99, DOI

[Fossati, G. 2008] Fossati, G.; Buckley, J. H.; Bond, I. H;...
Multiwavelength Observations of Markarian 421 in 2001 March: An Unprecedented View on the X-Ray/TeV Correlated Variability, ApJ, 2008, 677, 906, DOI

[Acciari, V. A 2011] Acciari, V. A.; Aliu, E.; Arlen, T.;...
TeV and Multi-wavelength Observations of Mrk 421 in 2006-2008, 2011, ApJ, 738, 25, DOI

[Aleksić, J. 2015] Aleksić, J.; Ansoldi, S.; Antonelli, L. A.;...
Unprecedented study of the broadband emission of Mrk 421 during flaring activity in March 2010,A&A, 2015, 578, A22, DOI

[Aleksić, J 2015] Aleksić, J.; Ansoldi, S.; Antonelli, L. A.;...
The 2009 multiwavelength campaign on Mrk 421: Variability and correlation studies, A&A, 2015, 576, A126, DOI

[Baloković, M. 2016] Baloković, M.; Paneque, D.; Madejski, G.;...
Multiwavelength Study of Quiescent States of Mrk 421 with Unprecedented Hard X-Ray Coverage Provided by NuSTAR in 2013, ApJ, 2016, 819, 156, DOI

[Sikora, M. 2000] [Sikora, M.; Madesjski, G.
On Pair Content and Variability of Subparsec Jets in Quasars, 2000, ApJ, 534, 109, DOI

[Acciari, V. A., 2014] Acciari, V. A.; Arlen, T.; Aune, T.;...
Observation of Markarian 421 in TeV gamma rays over a 14-year time span, Astroparticle Physics, 2014, 54 ,1-10.DOI

[Inoue, S. 1996] Inoue, S.; Takahara, F.

Electron Acceleration and Gamma-Ray Emission from Blazars, 1996, ApJ, 463, 555, ADS

[Sari, R. 2001] Sari, R.; Esin, A. A.

On the Synchrotron Self-Compton Emission from Relativistic Shocks and Its Implications for Gamma-Ray Burst Afterglows, 2001, ApJ, 548, 787,DOI

[Bloom, S. 1996] Bloom, Steven D. & Marscher, Alan P.

An Analysis of the Synchrotron Self-Compton Model for the Multi–Wave Band Spectra of Blazars, 1996, ApJ, 461, 657, DOI

[Marscher, A. P. 1985] Marscher, A. P.; Gear, W. K.

Models for high-frequency radio outbursts in extragalactic sources, with application to the early 1983 millimeter-to-infrared flare of 3C 273, 1985, ApJ, 298, 114, ADS

[Maraschi, L. 1992] Maraschi, L.; Ghisellini, G.; Celotti, A.

A jet model for the gamma-ray emitting blazar 3C 279, 1992, ApJ, 397,L5-L9. DOI

[Lindfors, E. J 2005] Lindfors, E. J.; Valtaoja, E.; Türler, M.

SSC mechanism in the gamma-ray blazar 3C 279, 2005, 440, 845, DOI

[Graff, P. 2008] Graff, P.; Georganopoulos, M.; Perlman, E.; Kazanas, D.

A multizone model for simulating the high-energy variability of TeV Blazars, 2008, ApJ, 689,68-78. DOI

[Dermer, C. D. 1992] Dermer, C. D.; Schlickeiser, R.; Mastichiadis A.

High-energy gamma radiation from extragalactic radio sources, 1992, A&A, 256, L27-L30, ADS

[Dermer, C. 1993] Dermer, C. D.; Schlickeiser, R.

Model for the High-Energy Emission from Blazars, 1993, ApJ, 416, 458, ADS

[Arbeiter, C] Arbeiter, C.; Pohl, M.; Schlickeiser, R.

The influence of dust on the inverse Compton emission from jets in Active Galactic Nuclei, 2002. A&A, 386, 415-426, DOI

[Harris, D. E. 2002] Harris, D. E. & Krawczynski, H.

X-Ray Emission Processes in Radio Jets, 2002, ApJ, 565,244-255, DOI

[Blazéjowski M. 2000] Blazéjowski M.; Sikora M.; ModerskI, R.; Madejski G.

Comptonization of infrared radiation from hot dust by relativistic jets in quasars, 2000, ApJ, 545,107-116,DOI

[Arbeiter, C 2002] Arbeiter, C.; Pohl, M.; Schlickeiser, R.

The influence of dust on the inverse Compton emission from jets in Active Galactic Nuclei, 2002, A&A, 386, 415-426, DOI

[Mannheim, K. 1993] Mannheim, K.

The proton blazar, A & A, 1993, 296, 67-76, arXiv

[Mücke, A. P., Protheroe, R.J. 2001] Mücke, A. P.; Protheroe, R.J.

A proton synchrotron blazar model for flaring in Markarian 501, 2001, Astroparticle Physics, 15, 1, 121-136, DOI

[Mücke, A., Protheroe, R. 2003] Mücke, A.; Protheroe, R.J.; Engel, R.; Rachen, J. P.; Stanev, T.

BL Lac Objects in the Synchrotron Proton Blazar Model, 2003, Astropart. Phys., 18, 593-613, DOI

[Aharonian, A. 2000] Aharonian, A.

TeV gamma rays from BL Lac objects due to synchrotron radiation of extremely high energy protons, 2000, New Astronomy, 5, 377, ADS

[Mannheim, K. 1989] Mannheim, K.; Biermann, P. L.

Photomeson production in active galactic nuclei, 1989, A&A, 221, 211-220, ADS

[Mannheim, K. 1992] Mannheim, K.; Biermann, P. L.

Gamma-ray flaring of 3C 279 : a proton-initiated cascade in the jet ?, 1992, A&A, 253, L21, ADS

[Rachen Jörg P. 2001] Rachen Jörg P.

Hadronic blazar models and correlated X-ray/ TeV flares, 2001, AIP Conference Proceedings, 515, 41, DOI

[Gutierrez, K 2006] Gutierrez, K.; Badran, H. M.; Bradbury, S. M.; Buckley, J. H.; Celik, O.; ...

MULTIWAVELENGTH OBSERVATIONS OF 1ES 1959+650, 1 YEAR AFTER THE STRONG OUTBURST OF 2002, 2006, ApJ 644:742–747, DOI

[Tachibana, Y. 2014] Tachibana, Y.; Kawai, N; Pike, P.

A Correlation Between Optical, X-ray, and Gamma-ray Variations in Blazar 3C 454.3, 5th Fermi Symposium: Nagoya, Japan : 20-24 Oct, 2014, NASA ADS

[Salpeter, E., 1964] Salpeter, E.

Accretion of interstellar matter by massive objects, Astrophysical Journal, 1964, 140,796, DOI

[Zeldovich, Ya. B., 1964] Zeldovich, Ya. B.

1964, Dokl. Akad. Nauk SSSR, 155, 67.

[Lynden-Bell, D. 1969] Lynden-Bell, D.

Galactic Nuclei as Collapsed Old Quasars, Nature, 1969, 223, 690, DOI

[Schwarzchild, K. 1916] Schwarzchild, K.

—- a) On the Gravitational Field of a Mass Point according to Einstein's Theory , Translation and foreword by S. Antoci and A. Loinger, 1999, ADS

—- b) On the Gravitational Field of a Sphere of Incompressible Fluid according to Einstein's Theory, Translation S. Antoci ,1999, ADS

[Blandford, Znajek 1977] Blandford, R. D., Znajek,R.L.

Electromagnetic extraction of energy from Kerr black holes, 1977, MNRAS, 179, 433, DOI

[Hovatta, T., Linfords, E. 2020] Hovatta, T., Linfords, E.

2019, Relativistic Jets of Blazars,New Astronomy Reviews 87, 101541, DOI

[Böttcher, M., 2001] Böttcher, M.

Leptonic Jet Models of Blazars: Broadband Spectra and Spectral Variability, 2001, ADS

[Cerruti, M. 2020] Cerruti, M.

Leptonic and Hadronic Radiative Processes in Supermassive-Black-Hole Jets, 2020, MDPI, DOI

[Sikora, M., 2011] Sikora, M.

Hadronic jet models today, 2011, Jets at all Scales Proceedings IAU Symposium No. 275, 2011, DOI

[Osterbrock, D. 2006] Osterbrock, Donald.

Astrophysics of Gaseous Nebulae and Active Galactic Nuclei. Second Edition. by D.E. Osterbrock and G.J. Ferland. Sausalito, CA: University Science Books, 2006.ADS

[COSMOS] COSMOS (2020, June) WEB

[Beckmann V. 2012] Beckmann, Volker and Shrader Chris

Active Galactic Nuclei textbook, WILEY-VCH Verlag GmbH & Co. KGaA, DOI

[Rybicki, G. 1986] George B. Rybicki

Radiative Processes in Astrophysics, Wiley-Link

[Longair, 1994] Longair, M.S.

High Energy Astrophysics. Volume 2. Stars, the Galaxy and the Interstellar Medium; Cambridge University Press: Cambridge, UK, 1994; Volume 2.

[Bettini, A. 2008] Alessandro Bettini

Introduction to Elementary Particle Physics-Cambridge University Press (2008)